ARTICLE

SIRT1 in the BNST modulates chronic stress-induced anxiety of male mice via FKBP5 and corticotropin-releasing factor signaling

Pu Hu[1,8✉], Yu Wang[2,8], Xiu-Hong Qi[1], Qing-Hong Shan[2], Zhao-Huan Huang[3,4], Peng Chen[2], Xiao Ma[1], Yu-Peng Yang[1], Dick F. Swaab[5], Benjamin A. Samuels[6], Zhi Zhang[1] and Jiang-Ning Zhou[2,7✉]

© The Author(s), under exclusive licence to Springer Nature Limited 2023

Although clinical reports have highlighted association of the deacetylase *sirtuin* 1 (*SIRT1*) gene with anxiety, its exact role in the pathogenesis of anxiety disorders remains unclear. The present study was designed to explore whether and how SIRT1 in the mouse bed nucleus of the stria terminalis (BNST), a key limbic hub region, regulates anxiety. In a chronic stress model to induce anxiety in male mice, we used site- and cell-type-specific in vivo and in vitro manipulations, protein analysis, electrophysiological and behavioral analysis, in vivo MiniScope calcium imaging and mass spectroscopy, to characterize possible mechanism underlying a novel anxiolytic role for SIRT1 in the BNST. Specifically, decreased SIRT1 in parallel with increased corticotropin-releasing factor (CRF) expression was found in the BNST of anxiety model mice, whereas pharmacological activation or local overexpression of SIRT1 in the BNST reversed chronic stress-induced anxiety-like behaviors, downregulated CRF upregulation, and normalized CRF neuronal hyperactivity. Mechanistically, SIRT1 enhanced glucocorticoid receptor (GR)-mediated CRF transcriptional repression through directly interacting with and deacetylating the GR co-chaperone FKBP5 to induce its dissociation from the GR, ultimately downregulating CRF. Together, this study unravels an important cellular and molecular mechanism highlighting an anxiolytic role for SIRT1 in the mouse BNST, which may open up new therapeutic avenues for treating stress-related anxiety disorders.

Molecular Psychiatry (2023) 28:5101–5117; https://doi.org/10.1038/s41380-023-02144-6

INTRODUCTION

Anxiety disorders affect nearly 18.1% of the global adult population [1]. Stress-induced anxiety is often comorbid with major depression or substance abuse, and poses a considerable social burden [2, 3]. Therefore, developing effective therapeutics is urgently needed.

Mammalian Sirtuin1 (SIRT1) is an NAD^+-dependent deacetylase that regulates various physiological functions, including cell stress responses, energy metabolism, aging and brain synaptic plasticity [4–6]. Growing evidence implicates dysfunction of SIRT1 in the pathogenesis of depression [7, 8] and anxiety-related disorders [9, 10]. Moreover, clinical genome-wide association studies (GWAS) have further linked single nucleotide polymorphism (SNP) variations in the human *SIRT1* gene (particularly rs10997870) [11] to an increased risk to develop anxiety-related disorders, while reduced SIRT1 levels in the amygdala have been linked to the susceptibility to develop anxiety under pain conditions [12]. However, the exact function of SIRT1 and the underlying mechanism in the pathology of anxiety disorder remains unclear.

As one essential node of the brain circuits involved in anxiety regulation [13], the forebrain bed nucleus of the stria terminalis (BNST) is a key stress-responsive region [14]. Its anatomical location and unique circuit characteristics have led to the idea that it is a major 'hub' in the limbic system to control anxiety response [15–17]. So far, however, it remains unknown whether and how SIRT1 in the BNST modulates anxiety-like behaviors. Here, we address this question in a widely used chronic unpredictable mild stress (CUMS) paradigm in mice, that effectively induces anxiety-like behavior [18, 19]. Due to the heterogeneous nature of the BNST [20], we focus on the oval nucleus (ovBNST), which is critical in controlling its information outflow [16].

We test the above hypothesis by combining mouse genetics, site- and cell-type-specific in vivo and in vitro manipulations, including protein analysis, electrophysiological and behavioral analysis, MiniScope calcium imaging and mass spectroscopy. Our data demonstrate that SIRT1 activation in the BNST reverses chronic stress-induced anxiety phenotype. We show this is mediated via downregulation of corticotropin-releasing factor

[1]Hefei National Research Center for Physical Sciences at the Microscale, Chinese Academy of Sciences Key Laboratory of Brain Function and Diseases, Division of Life Sciences and Medicine, University of Science and Technology of China, Hefei 230027, PR China. [2]Institute of Brain Science, The First Affiliated Hospital of Anhui Medical University, Hefei 230022 Anhui, China. [3]National Engineering Laboratory for Brain-inspired Intelligence Technology and Application, School of Information Science and Technology, University of Science and Technology of China, Hefei 230026 Anhui, China. [4]Institute of Artificial Intelligence, Hefei Comprehensive National Science Center, Hefei 230026, China. [5]Department of Neuropsychiatric Disorders, Netherlands Institute for Neuroscience, An Institute of the Royal Netherlands Academy of Arts and Sciences, Meibergdreef 47, 1105 BA Amsterdam, The Netherlands. [6]Department of Psychology, Rutgers University, Piscataway, NJ 08854, USA. [7]Center for Excellence in Brain Science and Intelligence Technology, Chinese Academy of Sciences, Shanghai 200072, PR China. [8]These authors contributed equally: Pu Hu, Yu Wang. ✉email: phu@ustc.edu.cn; jnzhou@ustc.edu.cn

Received: 8 July 2022 Revised: 2 June 2023 Accepted: 16 June 2023
Published online: 29 June 2023

(CRF), a 41-amino-acid peptide, which critically regulates hypothalamic-pituitary-adrenal (HPA) stress axis activity [21] and is also highly expressed in the BNST [20, 22]. Downregulation of CRF occurs via deacetylation of FK506 binding protein 51 (FKBP5), an inhibitory co-chaperone of the glucocorticoid receptor (GR) [23–26]. Deacetylation of FKBP5 led to its dissociation from the GR, which subsequently enhances CRF transcriptional repression. As activation of CRF in the BNST per se is known to be anxiogenic [18], our current findings revealed a novel molecular and cellular mechanism for how SIRT1 exerts the anxiolytic effects.

MATERIALS AND METHODS

Experimental mice

All procedures were performed in accordance with the guide for care and use of laboratory animals of National Institutes of Health standards, and approved by the Institutional Animal Care and Use Committee of University of Science and Technology of China.

Mice were group housed (average 5 per cage) under controlled conditions. They were randomly assigned to a control or a test group. Information of mice strains are listed in Table 1.

For behavioral experiments, testing order of experimental mice was randomized.

Details of experimental mice information are listed in the supplemental file. Only male mice were used in this study. Investigators were blind to the animal grouping information, or genetic background of mice, or drug treatment or viral-expression information, when performing experiments or analyzing results.

No statistical methods were used to predetermine sample size. Sample size of animals (with 6-10 mice per group) was based on previous experiments and publications [18, 27], which were sufficient to determine significance between test and control groups. Mice with obvious health problem (such as skin lesion, tumor, eye injury, or movement disabilities) were excluded from our analysis. For drug-infusion experiments, mice with mis-placed cannulae were excluded. For viral experiments, mice with virus mis-injections were excluded.

Chronic Unpredictable Mild Stress (CUMS) paradigm

Details of CUMS protocol [18] have been described before. Variable mild stressors include: daily bedding alterations (repeated sawdust changes, removal of sawdust, damp sawdust, substitution with 21 °C water), cage-tilting (45° angle), predator sounds (15 min), cage shift, alterations of the light/dark cycle, lights off for 180 min, and overnight food/water deprivation.

Animal grouping information are listed in the supplemental file.

Behavioral tests

Behavioral tests were performed between 9:00 am to 6:00 pm [28]. Tests include the elevated plus maze (EPM), open-field (OF) (both evaluate anxiety-like behavior) and social Interaction (SI) test [29, 30] (which evaluates social anxiety level). Animals with similar weight and age were grouped randomly, and the number of mice for each group was 6-10. For behavioral experiments, testing order of experimental mice was randomized.

For EPM test, mice were placed in the central arena of a black plus-shaped maze, and were left to explore for 5 min.

For OF test, apparatus consists of a black floor area (40.5 cm × 40.5 cm), with a 37.5 cm high transparent wall. Mice were placed in the center and monitored for 10 min.

For SI test, the apparatus is comprised of a rectangular, three-chamber box. Each chamber is 19 × 45 cm; the dividing walls are made from clear Plexiglas, with an open middle section, which allows free access to each chamber. Two identical containers will contain each mouse individually. General room lighting is 650 lux.

More details are described in the supplemental file. Data were measured by video recording and processed by EthoVision (Noldus, Wageningen, The Netherlands).

Description of the main methods used

Specifically, the expression levels of SIRT1 and CRF were measured by immunohistochemistry (IHC), real-time quantitative PCR (q-PCR) and western blot. Details for CRF staining information, and primers used are listed in the supplemental files and Table 1.

Photographs were taken with a confocal microscope (Zeiss 880 system, Germany). Immunoblots were quantified using ImageJ software (Wayne Rasband, NIH, MD).

The site and cell-type specific manipulations were performed with cannulae-assisted pharmacological method, and AAV virus-mediated gene delivery method combined with transgenic mice line (mainly *CRH-IRES*-cre mice). Viral details are listed in the supplemental file and Table 1.

All the drug-infused mice were confirmed *post-hoc* (typical correct example is shown in Fig. 2B). Activity of CRF neurons was monitored by in vivo MiniScope calcium imaging.

Molecular studies were performed with in vitro cell culture system, including BE2C cell line and HEK293 cell line, using plasmid-mediated overexpression or siRNA-mediated knocking down. GR-mediated CRF transcription was examined with hCRF promoter pGL3-based Luciferase reporter system.

For the protein co-immunoprecipitation (co-IP) assay, plasmids were transiently transfected into HEK293 cells. Details for plasmid information, siRNA sequences, co-IP steps, antibody information, FKBP5 acetylation quantification assay are listed in supplemental file and Table 1.

Possible lysine deacetylation sites on FKBP5 were analyzed with mass spectrometry.

AAV-mediated viral overexpression

Mice were injected with AAV-SIRT1-eGFP or AAV-DIO-SIRT1-eGFP virus, or their respective control viruses (Brain VTA ltd, Wuhan, China; titer 2 ×10^12 particles/ml) into the ovBNST. Information of viruses were listed in Table 1. The injection rate was 2 nl/s and the needle remained for additional 7-8 min to allow stable penetration. Next, mice were put into warm cage for 30 min recovery before placed back. More details are provided in the supplemental file.

Electrophysiological recordings in brain slices

Standard whole-cell voltage-clamp patch recording was performed [18, 27].

After sacrifice of mice, a block containing the BNST was submerged in cold (4 °C) oxygenated (95% O_2, 5% CO_2) high-sucrose artificial cerebrospinal fluid (aCSF). Coronal slices (250 μm) were cut at 4 °C and were transferred to an auxiliary chamber and kept at room temperature (25 °C) for 1 h until recording. Slice was transferred to recording chamber mounted on an upright fluorescent microscope (Olympus, BX51W1) and continually perfused with warm (35 °C) oxygenated aCSF. Targeted fluorescent neurons were viewed with an Olympus 40x lens.

More details are listed in the supplemental file.

Chromatin immunoprecipitation (ChIP) assay for mouse BNST tissue

A ChIP assay [31] was performed with commercial kit (17-295, Millipore, MA). Details are listed in Supplemental file.

Tissue western blot

Total protein was extracted from the BNST and stored at −80 °C. Samples were immuno-blotted with an anti-SIRT1 antibody (rabbit, 1:1000; 07-131, Millipore, MA); GAPDH was used as endogenous control.

Signals were detected with ECL chemiluminescence system (SuperSignal West Pico chemiluminescence Substrate, Pierce, IL) and imaged with myECL imager (Thermo Fisher Scientific, MA). Results were expressed as percentage of GAPDH.

In vitro BE(2)C cell culture & plasmid transfection for Q-PCR and hCRF promoter luciferase assay

Human neuroblastoma BE(2)C cells (which endogenously secrete CRF; purchased from Conservation Genetics CAS Cell Bank, Shanghai, China) were grown and maintained in high-glucose DMEM (12100-046, Gibco) supplemented with 10% FBS (Invitrogen, CA) [32]. Semi-confluent cells (70–80%) were transiently transfected with different plasmids using Lipofectamine 3000 reagents (L3000015, Invitrogen, CA).

Details for cell line and plasmids used are provided in the supplemental file and Table 1.

Table 1. Key resources table.

Reagent or resource	SOURCE	IDENTIFIER
Antibodies:		
CRF:	Bachem	T4037; RRID: AB_518252
SIRT1:	Millipore	07-131; RRID: AB_2188349
GAPDH:	KangChen, China	KC-5G5; RRID: AB_2631280
FKBP5:	SantaCruz	sc-271547; RRID: AB_10649040
Ac-K:	Sigma	SAB5200090
His:	LifeTein	LT0426
HA:	Sigma	H9658; RRID: AB_260092
Flag:	Sigma	F1804; RRID: AB_262044
CBP:	Sigma	SAB4500455; RRID: AB_10743822
IgG:	Beyotime, Shanghai, China	A7016
GR:	SantaCruz	sc-393232; RRID: AB_2687823
Goat-anti-rabbit Alexa 594:	Jackson Laboratories	111-585-003
Goat-anti-rabbit Alexa 488:	Jackson Laboratories	111-545-003
Goat-anti-mouse Alexa 594:	Jackson Laboratories	115-585-003
Goat-anti-mouse Alexa 488:	Jackson Laboratories	115-545-003
PCR primers:		
Mouse CRF:	All synthesized from Takara, Shanghai, China	forward: 5′-AGGAGGCATCCTGAGAGAAGT-3′; reverse: 5′-CATGTTAGGGGCGCTCTC-3′ (86 bp; intron spanned)
Mouse SIRT1:		forward: 5′-GATGCTGTGAAGTTACTGCAGGAGTG-3′; reverse: 5′-GAGGGTCTGGGAGGTCTGGGAAG-3′;
Mouse β-actin:		forward: 5′-TGTTACCAACTGGGACGACA-3′; reverse: 5′-GGGGTGTTGAAGGTCTCAAA-3′ (165 bp; intron spanned);
Human CRF:		forward: 5′-CATCTCCCTGGATCTCACCTTC-3′; reverse: 5′-AATAATCTCCATAGTTTCCTGTTG-3′;
Human β-actin:		forward: 5′-CCCAGCCATGTACGTTGCTA-3′; reverse: 5′-TCACCGGAGTCCATCACGAT-3′.
Virus Strains:		
AAV-CMV-DIO-SIRT1-eGFP:	All synthesized from BrainVTA ltd, Wuhan, China	Cat#PT-1799
AAV-CMV-DIO-SIRT1-DN-eGFP:		Cat#PT-1801
AAV-CMV-DIO-eGFP:		Cat#PT-0310
AAV-CMV-SIRT1-eGFP:		Cat#PT-1606
AAV-CMV-SIRT1-DN-eGFP:		Cat#PT-1607
AAV-Ef1α-mCherry-U6-Loxp-CMV-eGFP-loxp- shRNA (SIRT1):		Cat#PT-2224
AAV-Ef1α-mCherry-U6-Loxp-CMV-eGFP-loxp-shRNA (control scramble):		Cat#PT-0900
AAV-DIO-GCaMP6f:		Cat#PT-0106
AAV-CMV-DO-SIRT1-eGFP-WPRE (loxP):		Cat#PT-2225
AAV-CMV-DO-eGFP-WPRE (control):		Cat#PT-2226
Experimental Models		
Mice Strains:		
C57BL/6J:	Vital River, China	Cat#213
CRH-IRES-Cre mouse:	Jackson Laboratory	RRID: IMSR_JAX:012704
Ai14 reporter mouse:	Dr. Minmin Luo, NIBS, Beijing	RRID: IMSR_JAX:007914
Cell Lines:		
SK-N-BE(2)C:	Neuroblastoma Homo sapiens	RRID: CVCL_0529
HEK293T:	Homo sapiens	RRID: CVCL_0063
Plasmids:		
GRα-eGFP:	Sino Biological, Shanghai, China	hGRα-pCMV-eGFP

Table 1. continued

Reagent or resource	SOURCE	IDENTIFIER
FKBP5-OFP:	Sino Biological, Shanghai, China	pCMV3-C-His-FKBP5-OFPS-park
SIRT1-eGFP:	All Synthesized from BrainVTA ltd, Wuhan, China	rAAV-CMV-SIRT1-P2A-EGFP-WPRE-bGH-polyA
SIRT1-mCherry:		rAAV-CMV-SIRT1-P2A-mCherry-WPRE-bGH-polyA
SIRT1-DN-eGFP:	Synthesized from BrainVTA ltd, Wuhan, China	SIRT1-DN (H355Y) site mutation
pGL3 basic:	Promega	pGL3 basic; E1751
pGL3-nGRE-Luc-reporter:	All generated from TsingKe Ltd, Nanjing, China	pGL3-nGRE-Luc
His-FKBP5:		pCMV3-C-His-FKBP5
Flag-GRα:		hGRα-pCMV-GFP-N-Flag;
		hGRα-pCMV-N-Flag
HA-SIRT1:	All generated from TsingKe Ltd, Nanjing, China	pCDNA3.1-C-HA-SIRT1
HA-SIRT1-DN:		pCDNA3.1-C-HA-SIRT1-DN(H355Y)
HA-P300:	All Generated by TsingKe Ltd, Nanjing, China	pCMV-C-HA-P300
HA-CBP:		pCMV-C-HA-CBP
siRNA for HEK293 cells:		
siRNA against SIRT1:	GenePharma, Shanghai, China	Sense: 5′-CCCUGUAAAGCUUUCAGAA(dTdT)-3′; antisense: 5′-UUCUGAAAGCUUUACAGGG(dTdT)-3′
control scramble siRNA:	GenePharma, Shanghai, China	Sense: 5′-UUCUCCGAACGUGUCACGUTT-3′; antisense: 5′-ACGUGACACGUUCGGAGAATT-3′
DNA sequence:		
GR-binding site 1 mutation:	All synthesized by TsingKe Ltd, Nanjing, China	5′-GAATTC-3′
GR-binding site 2 mutation:		5′-GAATTC-3′
GR-binding site 3 mutation:		5′-GAATTC-3′
Drugs:		
SRT2104:	Selleckchem	S7792
EX527:	Selleckchem	2780
CRF:	MedChemExpress	HY-P0086
Dexamethathone:	Sigma	D1756
Chromatin immunoprecipitation (ChIP) assay kit:		
ChIP kit:	Millipore	17-295
SIRT1 Enzyme Assay Kit:		
SIRT1 Direct Fluorescent Screening Assay Kit:	Cayman	10010401
Patch Clamping Setup:		
Microscope:	Olympus	BX51W1
Axopatch 700B amplifier:	Molecular Devices	Axopatch700B
Digidata 1322A Data	Molecular Devices	Digidata 1332A
Acquisition System:		
Software and Algorithms:		
ImageJ (Fiji) software:	National Institute of Health	
MATLAB:	MATLAB 2020b, Mathworks	
GraphPad Prism 7:	GraphPad Software	
CNMF-E:	https://github.com/zhoupc/CNMF_E	
pCLAMP software:	Molecular Devices	
Python software:	Python Software Foundation	

Cell culture and plasmid transfection for protein co-immunoprecipitation (co-IP)

HEK293T cells (purchased from Conservation Genetics CAS Cell Bank, Shanghai, China) were cultured in DMEM medium (Sigma, MO), supplemented with 10% fetal bovine serum (FBS) (Gibco, NY). For the protein co-IP assay, plasmids were transiently transfected with Lipofectamine 3000 (Invitrogen, CA), using Pierce co-IP kit (88805, ThermoScientific, IL). Details for cell line and plasmids used are provided in the supplemental file and Table 1.

Mass spectrometry

Cultured HEK293T cells expressing His-FKBP5 were transfected with control or SIRT1-siRNA. 48 h later, cells were lysed with RIPA lysis buffer. FKBP5 protein bands were processed for LCMSMS mass spectrometry (Q Exactive, Thermo Fisher; Easy-nLC 1000) (Shanghai Applied Protein Technology Co. Ltd, Shanghai, China) and detection of possible acetylation sites. Details were listed in the supplemental files.

In vivo miniature fluorescence microscope (MiniScope) calcium imaging recording

For calcium imaging of BNST CRF neurons in vivo, we applied the MiniScope technique [33, 34]. Mice were exposed to an established elevated platform standing (EPS) behavioral paradigm [35], which elicits acrophobia-related stress and anxiety. Details for GCaMP virus injection, GRIN Lens coating and implantation, calcium signal statistics and behavioral signal coupling, and ROI selection, and constrained non-negative matrix factorization framework (CNMF-E)-based data analysis pipeline (https://github.com/zhoupc/CNMF_E) [36] are listed in the supplemental file.

Quantification and statistical analysis

All data are presented as mean ± SEM. Statistical analysis were conducted with GraphPad Prism 6.0 (La Jolla, CA). Sample sizes are indicated in the figure legends. The numbers N indicate the number of biological repeats (animals or tissue or cell samples). For behavioral and IHC results, data were analyzed with Student's *t* test, or ANOVA (analysis of variance). For mEPSCs, data were analyzed with Mini Analysis (Synaptosoft, NJ) and compared using Student's *t* test.

The normality and variance of data distributions were analyzed by Shapiro–Wilk test and F test, respectively. For data that did not conform to normality or homoscedasticity, non-parametric tests (Mann–Whitney U tests) were applied. For normally distributed data, two-tailed t tests were used to assess difference between two groups with equal variances; for two groups with unequal variances, two-tailed t-tests with Welch's correction were applied. For analysis of three or more groups, two-way ANOVA test (followed by post hoc Tukey test) was applied to analyze difference with two factors; one-way ANOVA test (followed by Bonferroni post hoc test) was applied to analyze difference with one factor.

For MiniScope data, repeated measures ANOVA was applied followed by post-hoc Tukey test (before vs. after EPS), with group effect and EPS effect as independent parameters. Three parameters were analyzed: 1) average calcium peak amplitude, 2) average signal area under the peak, and 3) average calcium transient event frequency. Differences were considered significant when $p < 0.05$.

RESULTS

Increased CRF in parallel with decreased SIRT1 expression in the BNST from chronically stressed anxiety model mice

Following 6 weeks of exposure to chronic unpredictable mild stress (CUMS) (Fig. 1A), stressed C57 mice displayed a typical anxiety-like phenotype, as demonstrated by results from the elevated plus maze (EPM; trace example: Fig. 1B) (Fig. 1C, D) and open field (OF; trace example: Fig. 1E) (Fig. 1F–H) tests, including decreased duration (C: $p = 0.002$) and entry (D: $p = 0.017$) in open arms, decreased traveling distance (F: $p = 0.010$), duration (G: $p = 0.018$), and entry frequency (H: $p = 0.046$) in the center. These data indicate that CUMS increased avoidance behavior and heightened overall anxiety. No differences were found between CUMS and Control mice in either total arm entries in EPM test or total distance in the OF test (Supplementary Fig. S1A, B), indicating CUMS did not affect locomotion per se.

Furthermore, the 3-chamber social interaction (SI) was applied to examine the levels of social anxiety [37] (tracking trace example shown in Fig. 1I–J). In contrast to Control mice (Session 1: $p < 0.01$; Session 2: $p < 0.01$), in Session 1 (sociability test; Fig. 1K), CUMS mice showed no differences in contact duration with Stranger 1 vs. the empty cage control ($p = 0.270$); in Session 2 (social novelty preference test; Fig. 1L), they showed no differences in contact duration with novel Stranger 2 vs. familiar Stranger 1 ($p = 0.162$). Hence, CUMS mice displayed enhanced social anxiety level. Together with the EPM and OF results, we conclude that they display a typical anxiety-like behavioral phenotype.

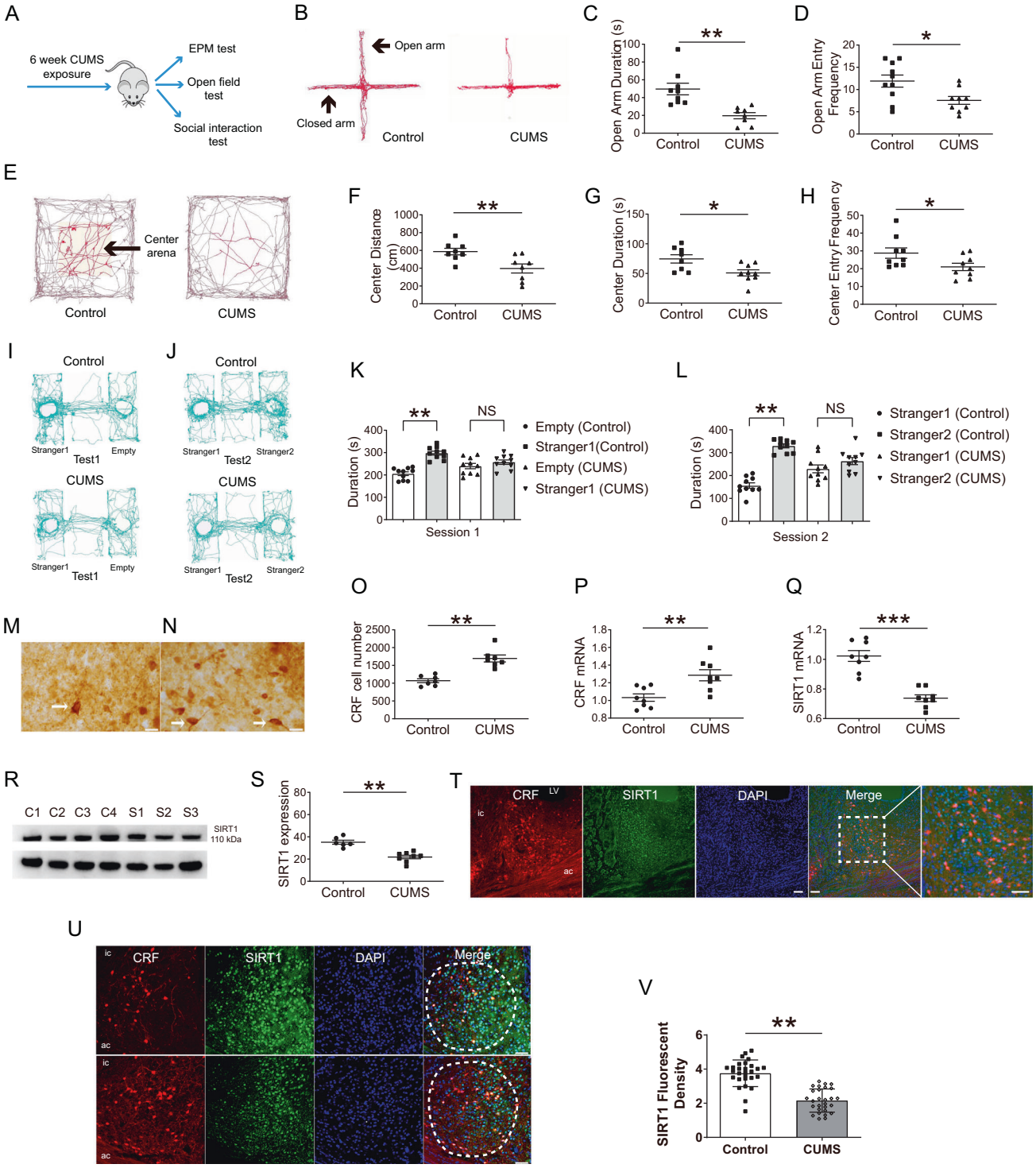
The stress neuropeptide CRF is abundantly expressed in the ovBNST [20], where it mediates chronic stress-induced maladaptive behaviors [18]. A representative example of CRF expression in the BNST at high-magnification is shown from Control (Fig. 1M) and CUMS mice (Fig. 1N). A representative comparison of CRF immunostaining pattern in the BNST from CUMS vs. Control mice was shown in Supplementary Fig. S1C, D. As expected, CUMS mice display an increased number of CRF-immunopositive cells compared to controls (Fig. 1O; $p < 0.01$), which was confirmed by QPCR (Fig. 1P; $p = 0.006$). In parallel, a decrease in SIRT1 mRNA level was found in CUMS group (Fig. 1Q; $p < 0.001$) which were further confirmed by western blot analysis (Fig. 1R, S; $p < 0.01$). These data indicate that CUMS increases the expression of CRF and decreases SIRT1 expression in the BNST. To study possible co-localization pattern of SIRT1 and CRF in the BNST, we analyzed BNST slices from *CRH-IRES-Cre;Ai14* reporter mice [34] (validity was shown in Supplementary Fig. S1E–K). Almost all CRF-tdTomato cells co-localized with $SIRT1^+$ cells, as shown in Fig. 1T. The average percentage of CRF^+ cell number relative to the total $SIRT1^+$ cell number in the BNST is shown in Supplementary Fig. S1L. Together, CUMS induces a robust anxiety-like phenotype, accompanied by CRF upregulation and SIRT1 downregulation in the BNST.

To further compare the expression intensity of SIRT1 in BNST CRF cells under stress vs. control condition, we performed double-immunofluorescence staining (Fig. 1U). Quantification results show that under CUMS condition, SIRT1 fluorescent intensity in CRF cells was significantly decreased (Fig. 1V; $p < 0.01$).

Pharmacological activation or viral-mediated local overexpression of SIRT1 in the ovBNST reverses the anxiety phenotype of CUMS mice

Since CUMS downregulates SIRT1 expression, we hypothesized that pharmacological activation of SIRT1 may affect the anxiety phenotype. Through cannulation that targets the ovBNST region-specifically, we infused the SIRT1-selective agonist SRT2104 [8] into ovBNST for 7 days during the last week of the CUMS or control paradigm (Fig. 2A) for CUMS or Control mice. Confirmation example of correct cannulae position was shown in Fig. 2B.

Interestingly, when SRT2104 was infused into the BNST, the anxiety-like behaviors of CUMS mice were alleviated as compared with its saline. The results in the EPM were shwon in Fig. 2C, D (C: for duration stay, ANOVA shows a group effect: $F(1,24) = 24.434$, $p = 0.000$; but not treatment effect: $F(1,24) = 2.925$, $p = 0.1$; nor interaction: group x treatment: $F(1,24) = 1.583$, $p = 0.220$; D: for entry frequency, ANOVA shows both group effect: $F(1,24) = 54.321$, $p = 0.012$; and treatment effect: $F(1,24) = 4.620$, $p = 0.042$; and interaction effect: group x treatment: $F(1,24) = 8.082$, $p = 0.009$). The results of OF test were shown in Fig. 2E–G (E: for center distance, ANOVA shows a group effect: $F(1,24) = 14.211$, $p = 0.001$, and an interaction between group x treatment: $F(1,24) = 6.222$, $p = 0.02$; but not treatment effect: $F(1,24) = 2.551$, $p = 0.123$; F: for center duration, ANOVA shows both group effect: $F(1,24) = 11.327$, $p = 0.003$; and treatment effect: $F(1,24) = 4.464$, $p = 0.045$; group x treatment: $F(1,24) = 8.614$, $p = 0.007$; G: for center entry frequency, ANOVA shows group effect: $F(1,24) = 8.374$, $p = 0.008$; and the interaction



effect, group x treatment: $F(1,24) = 6.290$, $p = 0.019$; but not treatment effect: $F(1,24) = 3.538$, $p = 0.072$). For all these parameters that we examined, no difference was found between the Control vs Control+SRT2104 groups ($p > 0.05$ for all three parameters). These results indicate that SRT2104 reduced the avoidance behavior in stressed mice, but did not affect behavior in control mice. Similarly, SRT2104 treatment also improved the social anxiety level of CUMS mice in the SI tests (Fig. 2H, I). SRT2104-infused mice showed increased contact duration towards Stranger 1 mice vs. empty cage ($p < 0.01$) in SI test 1, and towards Stranger 2 vs. Stranger 1 mice ($p < 0.01$) in SI test 2. Effects of SRT2104 on the social interaction properties of control mice were shown in Supplementary Fig. S2A, B. Neither SRT2104 infusion nor SIRT1-overexpression had significant effect on the overall locomotion capability of control or CUMS mice (Supplementary Fig. S2C–F).

In contrast to the effects of agonist, infusion of the SIRT1 antagonist EX527 had no effects on the anxiety-like phenotype of CUMS-exposed mice (Supplementary Fig. S3; likely due to a ceiling effect of the CUMS exposure). Confirmation of the tissue viability was shown in Supplementary Fig. S4. Taken together, we show that pharmacological activation of SIRT1, but not inactivation,

Fig. 1 Anxiety-like behaviors accompanied by increased corticotropin-releasing factor (CRF) and decreased SIRT1 expression in the BNST of chronic unpredictable mild stress (CUMS)-exposed mice. A Experimental schematics. C57 mice were subjected to 6-week CUMS for examination of anxiety-related behaviors. **B** Tracking trace examples in EPM (elevated plus maze) test. **C**, **D** Duration of stay and entry frequency in the open arms of EPM test compared for CUMS and unstressed Control group (both $n = 9$-10). **E** Tracking trace examples in open field (OF) test. **F**–**H** Traveling distance, duration stay and entry frequency within center of OF test, compared for CUMS and unstressed Control mice (both $n = 8$-9). **I**, **J** Tracking trace examples in the social interaction (SI) test. **K**, **L** In the SI test, comparison of contact duration towards Stranger 1 mice vs. empty cage Control (SI test1), towards Stranger 2 vs. Stranger 1 mice (SI test2), for CUMS ($p > 0.05$ for both tests) vs. unstressed Control mice (both tests: $p < 0.01$) ($n = 9$-10 in both groups). **M**, **N** Amplified example of CRF-immunopositive cells (pointed by white arrows; scale bar: both 20 μm) in the BNST from Control (M) vs. CUMS (**N**) mice. **O** Increased CRF^+ cell number was found in the BNST from CUMS vs. Control (both $n = 7$) mice. **P**, **Q** CUMS resulted in upregulation of *CRF* (P) and downregulation of *SIRT1* (Q) mRNA expression in the mouse BNST ($n = 8$ in both groups). **R:** Western blot bands example of SIRT1 protein expression in the BNST from Control (C1–C4; $n = 4$ shown) vs. CUMS (S1–S3; $n = 3$ shown) mice. GAPDH was used as internal control. **S** Comparison of normalized protein density of SIRT1 expression in the BNST from CUMS ($n = 8$; 21.9 ± 1.6% of GAPDH) vs. Control mice ($n = 6$; 35.2 ± 1.79% of GAPDH) ($p < 0.01$). **T** Co-localization pattern (right; merged) of CRF-tdTomato (red; left), SIRT1 fluorescence (green) and DAPI (blue) in the BNST from *CRH-IRES-Cre*;Ai14 reporter mice (scale bar: all 50 μm). **U** SIRT1 (green) co-localization pattern with CRF-positive (red) cells under Control (upper panels) vs. CUMS condition (bottom panels). Scale bar: both 50 μm. DAPI (blue) shows the nucleus. White circle highlights the boundary of oval nucleus region of BNST (ovBNST). **V** Comparison of average SIRT1 immunofluorescent density in BNST CRF neurons between CUMS and control group of mice. Data were collected from $n = 5$ mice per group. For each mouse, 5-6 sections were analyzed, which were located along the rostral to caudal axis of BNST. Each data point represents average fluorescent density value in each one of the sections that are taken into analysis. ic internal capsule, ac anterior commissure, LV lateral ventricle. *$p < 0.05$; **$p < 0.01$; ***$p < 0.001$; NS non-significant.

selectively in the BNST, alleviates the anxious phenotype of chronically stressed mice.

We further examined the effect of local, viral-mediated SIRT1 overexpression (OE), selectively in the ovBNST, of CUMS mice (Fig. 2J). To this end, AAV-SIRT1-eGFP was injected into the ovBNST (Fig. 2K) at the start of the 4th week of the CUMS paradigm. Interestingly, as compared with control virus (AAV-Con)-overexpressed mice, (Fig. 2L, M), SIRT1-OE mice spent more time ($p = 0.007$) and entered more frequently ($p = 0.009$) into open arms in EPM test than that of CUMS mice. For open arm duration stay (Fig. 2L), group effect: $F(1,29) = 30.007$, $p = 0.000$; treatment effect: $F(1,29) = 7.955$, $p = 0.037$; group x treatment: $F(1,29) = 1.002$, $p = 0.325$. For open arm entry frequency (Fig. 2M), group effect: $F(1,30) = 8.602$, $p = 0.006$; treatment effect: $F(1,24) = 5.556$, $p = 0.025$; group x treatment: $F(1,30) = 3.131$, $p = 0.087$. In the OF (Fig. 2N–P), SIRT1-OE mice traveled farther ($p = 0.001$), spent more time ($p = 0.021$), and entered more frequently ($p = 0.005$) into the center arena than CUMS mice. For center traveling distance (Fig. 2N), group effect: $F(1,29) = 8.244$, $p = 0.008$; treatment effect: $F(1,29) = 0.617$, $p = 0.439$; group x treatment: $F(1,29) = 3.650$, $p = 0.066$. For traveling duration in center (Fig. 2O), group effect: $F(1,29) = 3.456$, $p = 0.073$; treatment effect: $F(1,29) = 1.985$, $p = 0.170$; group x treatment: $F(1,29) = 2.480$, $p = 0.126$. For center entry frequency (Fig. 2P), group effect: $F(1,29) = 4.324$, $p = 0.012$; treatment effect: $F(1,29) = 7.581$, $p = 0.01$; group x treatment: $F(1,29) = 5.062$, $p = 0.032$.

Moreover, in SI test, as compared with CUMS mice over-expressing control vector, SIRT1-OE mice demonstrated less social anxiety level (Fig. 2Q, R). They showed increased contact duration towards Stranger 1 mice vs. empty cage in SI test 1 ($p < 0.01$), and towards Stranger 2 vs. Stranger 1 in SI test 2 ($p < 0.01$). Together, overexpressing SIRT1 in the ovBNST effectively alleviated the anxiety-like phenotype of CUMS mice.

We next examined CRF mRNA expression. Interestingly, decreased CRF mRNA levels were found in CUMS+SIRT1-OE vs. CUMS mice ($p = 0.003$) (Fig. 2S). We also verified SIRT1 protein expression level in the BNST among different vector-treated groups (Fig. 2T, U). While SIRT1 expression were significant higher in SIRT1-OE mice than its control vector in CUMS group ($p = 0.002$), there was no difference in SIRT1 protein level between CUMS mice and those overexpressing control vector ($p = 0.502$), nor between CUMS mice overexpressing SIRT1 and those over-expressing enzyme-inactive SIRT1-DN ($p = 1.000$).

Finally, we tested SIRT1 enzyme activity. Compared to control mice, CUMS-exposed mice exhibited a reduced enzyme activity ($p = 0.001$) (Fig. 2V), which was upregulated in SIRT1-OE ($p = 0.004$) or SRT2104-treated mice ($p = 0.035$), but not in SIRT1-DN-OE mice ($p = 0.383$). SRT2104 treatment had no significant effect on SIRT1 enzyme activity for control mice ($p = 0.445$). Together, overexpression of SIRT1 in the BNST restored SIRT1 enzyme activity of CUMS mice.

Downregulation of CRF is required for the anxiolytic phenotype induced by SIRT1 overexpression

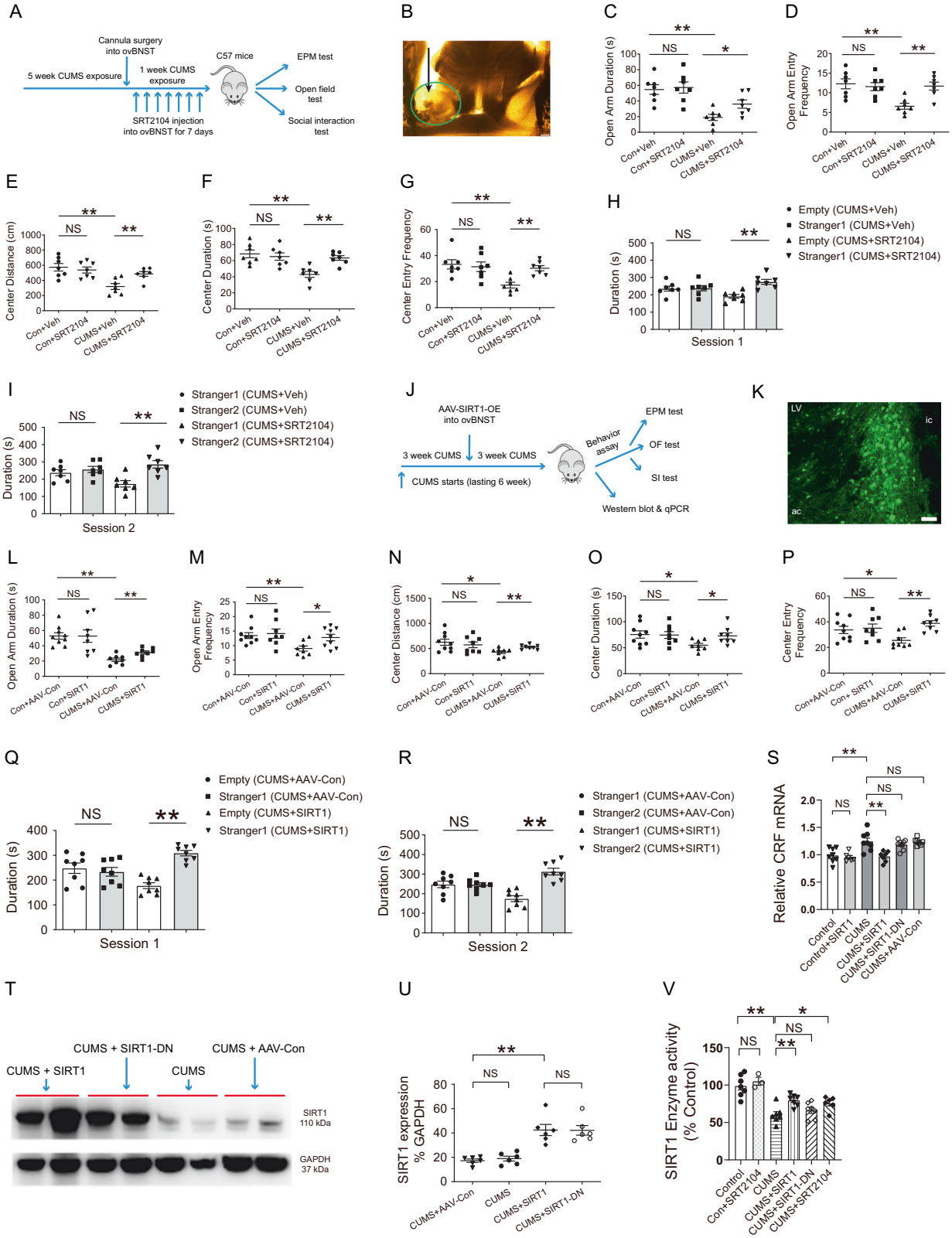
We next asked whether selective overexpression of SIRT1 in the CRF neurons in the ovBNST could be anxiolytic. To this end, we injected AAV-DIO-SIRT1-eGFP into the ovBNST of *CRH-IRES-Cre*;Ai14 reporter mice at the beginning of the 4th week of CUMS (Fig. 3A). Most SIRT1-eGFP-infected cells co-localized with CRF-tdTomato (Fig. 3B).

Interestingly, these SIRT1-OE mice displayed reduced anxiety-like behavior in both the EPM task (Fig. 3C, D) (CUMS vs. CUMS +SIRT1: open arm duration stay: $p = 0.004$; entry frequency: $p = 0.001$) and OF task (Fig. 3E–G) (CUMS vs. CUMS+SIRT1: center distance: $p = 0.035$; center duration: $p = 0.022$; center entry frequency: $p = 001$) as compared to CUMS mice. Furthermore, in the SI tests, SIRT1-OE mice displayed reduced social anxiety level (Fig. 3H, I). (both $p < 0.01$, contact duration towards Stranger 1 vs. empty cage in SI 1 test, and in SI 2 test, towards Stranger 2 vs. Stranger 1). Taken together, selective overexpression of SIRT1 within BNST CRF neurons of CUMS mice is sufficient to produce an anxiolytic effect.

While overexpressing the enzyme-inactive AAV-SIRT1-DN-eGFP mutant in the C57 CUMS mice had no effect (Supplementary Fig. S5), overexpressing enzyme-inactive SIRT1-DN (Supplementary Fig. S6), or control vector in CRF neurons (supplementary Fig. S7), or overexpressing SIRT1 in the non-CRF cells (Supplementary Fig. S8) of *CRH-IRES-Cre*;Ai14 reporter mice all had no effect. By contrast, knocking down SIRT1 in the CRF neurons within ovBNST using shRNA in stress-free naïve mice rather produced an anxiety-like phenotype (Supplementary Fig. S9), suggesting that SIRT1 in the BNST may play a tonic anxiolytic role.

Chronic stress is further known to potentiate excitatory synaptic transmission in ovBNST CRF neurons [18] via enhanced CRF signaling. We therefore next explored the effect of SIRT1-OE on excitatory synaptic transmission. CRF neurons were visualized and labeled in the BNST slices of *CRH-IRES*-Cre;Ai14 reporter mice (Fig. 3J). Typically, they were patched with Neurobiotin 488 (green; through internal solution) to confirm its identity *post-hoc* (merged; yellow).

As expected (Fig. 3K), an increased mEPSC amplitude was found in CUMS vs. Control mice (Fig. 3L; $p < 0.01$), which was normalized in stressed SIRT1-OE mice ($p < 0.01$). SIRT1-OE in Control mice had



no effect ($p = 0.442$, Control vs. Control+SIRT1), and mEPSC frequency showed no differences across the four groups (Fig. 3M; $p > 0.05$ for all these parameters). This suggests that SIRT1-OE normalizes the CUMS-potentiated excitatory synaptic transmission in CRF neurons in the BNST.

We next explored whether the anxiolytic effect of SIRT1 persisted following an exogenous administration of CRF into the ovBNST. To this end, first we overexpressed (OE) AAV-DIO-SIRT1 into ovBNST at the beginning of 4th week during 6-week CUMS procedure in CRH-Cre mice, then we implanted cannulae (Fig. 3N),

Fig. 2 Pharmacologically activating SIRT1 or viral-mediated local overexpression of SIRT1 in the BNST reverses the anxiety phenotype of CUMS mice. A Experimental schematics outline. SIRT1-selective agonist SRT2104 was infused (10 μM in 0.5 μl saline) into ovBNST of CUMS or Control mice through cannulae and delivered for 7-day during the last week of CUMS procedure. **B** Bright-field example of mouse BNST after cannulae injection for *post-hoc* position confirmation. The oval nucleus of BNST (ovBNST) is highlighted with a green circle. Black arrow points to the correct position of the cannulae tip, which should locate just above the border or within the boundary of the mouse ovBNST. Scale bar: 100 μm. **C**, **D** Compared with vehicle (Veh; DMSO) infusion, SRT2104 infusion resulted in increased duration stay and entry frequency in the open arms of EPM test for CUMS mice. No change was found for Control mice after SRT2104 infusion. $N = 7$ mice per group. **E**–**G** After SRT2104 infusion, for CUMS mice, traveling distance, duration and entry frequency in the OF center were all increased. No change was found for Control mice after SRT2104 infusion. $N = 7$ mice per group. **H**, **I** After SRT2104 infusion, CUMS mice (CUMS+SRT2104 group) displayed increased contact duration towards Stranger 1 mice vs. empty cage in SI test 1, and towards Stranger 2 vs. Stranger 1 mice in SI test 2, in contrast with vehicle infusion (CUMS+Veh group). $N = 7$ mice per group. **J** Schematics illustrating AAV-SIRT1-eGFP overexpression (OE) in the BNST of C57 mice at the beginning of the 4th week during CUMS procedure. 3 weeks later, anxiety-related behaviors were tested. **K** Example of AAV-SIRT1-eGFP fluorescence in the ovBNST (scale bar: 50 μm). ic internal capsule, ac anterior commissure, LV lateral ventricle. **L**, **M** In the EPM open arms, SIRT1-OE resulted in increased duration stay and entry frequency, as compared with CUMS mice. No change was found for Control mice after SIRT1 overexpression. $N = 8$-9 mice per group. **N**, **P** In the OF center, SIRT1-OE resulted in increased traveling distance, duration and entry frequency, as compared with CUMS mice. No change was found for Control mice after SIRT1 overexpression. $N = 8$-9 mice per group. **Q**, **R** SIRT1-OE resulted in increased contact duration towards Stranger 1 mice vs. empty cage in SI test 1, and towards Stranger 2 vs. Stranger 1 in SI test 2, as compared with CUMS mice. No difference was found for CUMS mice overexpressing Control vector. $N = 8$ mice per group. **S** CRF mRNA expression from the BNST was compared among different groups of mice, including Control mice, Control mice overexpressing SIRT1 vector (Con+SIRT1), CUMS mice, CUMS mice overexpressing SIRT1 vector (CUMS+SIRT1) or mutant SIRT1-DN vector (CUMS+SIRT1-DN), or Control vector (CUMS+AAV-Con). $N = 7$-8 mice per group. Data are presented relative to Control group (set as 1.0). **T** Example of SIRT1 western bands from the same four groups of mice as described above ($n = 2$ bands from each group were shown). GAPDH was used as internal control. **U** Comparison of average SIRT1 protein expression density (% GAPDH) in the BNST among the CUMS+AAV-Con, CUMS, CUMS+SIRT1 and CUMS+SIRT1-DN groups of mice ($n = 6$ per group). **V** Quantification of average SIRT1 enzyme activity (measured with the SIRT1 fluorescent screening assay kit) in the BNST, as compared from non-stressed Control group, SRT2104-infused control group (Con+SRT2104), CUMS group, SIRT1-overexpressed CUMS group (CUMS+SIRT1), CUMS group of mice overexpressing SIRT1-dominant negative mutant (CUMS +SIRT1-DN group), and SRT2104-infused CUMS group (CUMS+SRT2104). Data are presented relative to the non-stressed Control group (set as 100%). $N = 6$-7 mice per group. *$p < 0.05$; **$p < 0.01$; NS non-significant.

via which CRF (1 nM) was infused for 7 days during the last week of CUMS. As a control, we also included a saline-treated SIRT1-OE group (CUMS+SIRT1+Saline), and examined anxiety-related behaviors for these 4 groups of mice. Strikingly, when CRF was infused for 7 days, the anxiolytic effect of SIRT1-OE was abolished, as compared with saline-infused group, reflected by results in EPM (Fig. 3O, P) and OF (Fig. 3Q–S) tests, as well as in SI tests (Fig. 3T, U). Specifically, significant decreases in the above parameters were found in CUMS+SIRT1+CRF group compared with CUMS +SIRT1+Saline group: in the EPM open arms, duration stay: $p = 0.001$ (Fig. 3O); entry frequency: $p = 0.023$ (Fig. 3P); in the OF center, traveling distance: $p = 0.021$ (Fig. 3Q); duration: $p = 0.038$ (Fig. 3R); and center entry frequency: $p = 0.007$ (Supplementary Fig. 3S). In the SI test, CUMS+SIRT1+CRF group showed no significant difference towards Stranger 1 mice vs. empty cage ($p = 0.259$; Fig. 3T), and towards Stranger 2 vs. Stranger 1 mice ($p = 0.710$; Fig. 3U) as well. These were in contrast with CUMS +SIRT1+Saline group ($p < 0.01$ in both SI tests).

Together, the anxiolytic effects of SIRT1-OE were abolished when CRF was administered. Therefore, CRF downregulation is required for the anxiolytic effect of SIRT1.

SIRT1 overexpression normalizes the hyperactivity of CRF neurons in the BNST of chronically stressed mice

To verify whether CRF neurons in the BNST also contribute functionally to the anxiety-like behavior in vivo, we utilized a MiniScope method (Fig. 4A) in freely moving animals.

AAV-DIO-GCaMP6f was injected into the ovBNST of *CRH-IRES-Cre* mice, and the lens localization was confirmed post-hoc (Fig. 4B). Figure 4C shows a fluorescent example of amplified GCaMP6f-eGFP signal. Real-time GCaMP calcium activity was monitored before and after subjection of the mice to a 5 min of elevated platform (EPS) exposure as anxiogenic stimulus (Fig. 4D). Calcium signals were extracted by an extended CNME-E-based framework (demonstrating a unique advantage of improved source accuracy) [36]. Figure 4E, F shows a typical calcium image and a representative example of enlarged calcium intensity from Control mice. Representative calcium traces were compared among different CRF neurons at baseline (Fig. 4G) and after EPS (Fig. 4H).

Typical calcium images, representative intensity examples and calcium traces (Z-score values plotted against time and compared at baseline and after EPS) are shown from CUMS mice (Fig. 4I–L) and CUMS+SIRT1 mice (Fig. 4M–P).

Next, we quantified calcium activity in different groups. A repeated-measures ANOVA showed both a group effect ($F(2,259) = 43.903$, $p < 0.001$) and EPS effect ($F(1,259) = 181.03$, $p = 0.001$). Interestingly, for both control and CUMS mice, EPS induced an increase in calcium amplitude compared to baseline (both $p < 0.01$) (Fig. 4Q). After EPS, the average peak amplitude was even higher in CUMS vs. Control mice. In contrast, the average amplitude showed no change for CUMS+SIRT1 mice after EPS compared with under baseline condition ($p = 0.070$).

We also compared the frequency of calcium events (Fig. 4R) that increased following EPS, exclusively in CUMS mice ($p < 0.01$ under baseline vs. after EPS). Repeated-measures ANOVA showed both a group effect ($F(2,230) = 6.219$, $p = 0.002$) and EPS effect ($F(1,230) = 28.497$, $p = 0.001$). No change in frequency was observed in Control mice ($p = 0.234$) or CUMS+SIRT1 mice ($p = 0.548$) after EPS.

For the average signal area (Fig. 4S), repeated-measures ANOVA revealed no group effect ($F(2,167) = 0.509$, $p > 0.05$) or EPS effect ($F(1,259) = 1.46$, $p > 0.05$). There were no changes after EPS exposure compared with baseline in either of the three groups: for Control group, $p = 0.911$; for CUMS group, $p = 0.762$; for CUMS +SIRT1 group, $p = 0.630$.

BNST CRF neurons were furthermore classified (Supplementary Fig. S10) according to their calcium response patterns. We found CUMS mice displayed an increased percentage of on-responder CRF neurons (hyperactivity), which was normalized by SIRT1 overexpression. Taken together, SIRT1 normalizes the hyperactivity of CRF neurons in the BNST of CUMS mice induced by EPS.

SIRT1 enhances GR-mediated transcriptional repression of CRF in vitro

The above results emphasized a key role of downregulation of CRF here in mediating the anxiolytic effects of SIRT1. Given that CRF transcription is subject to negative regulation of glucocorticoid

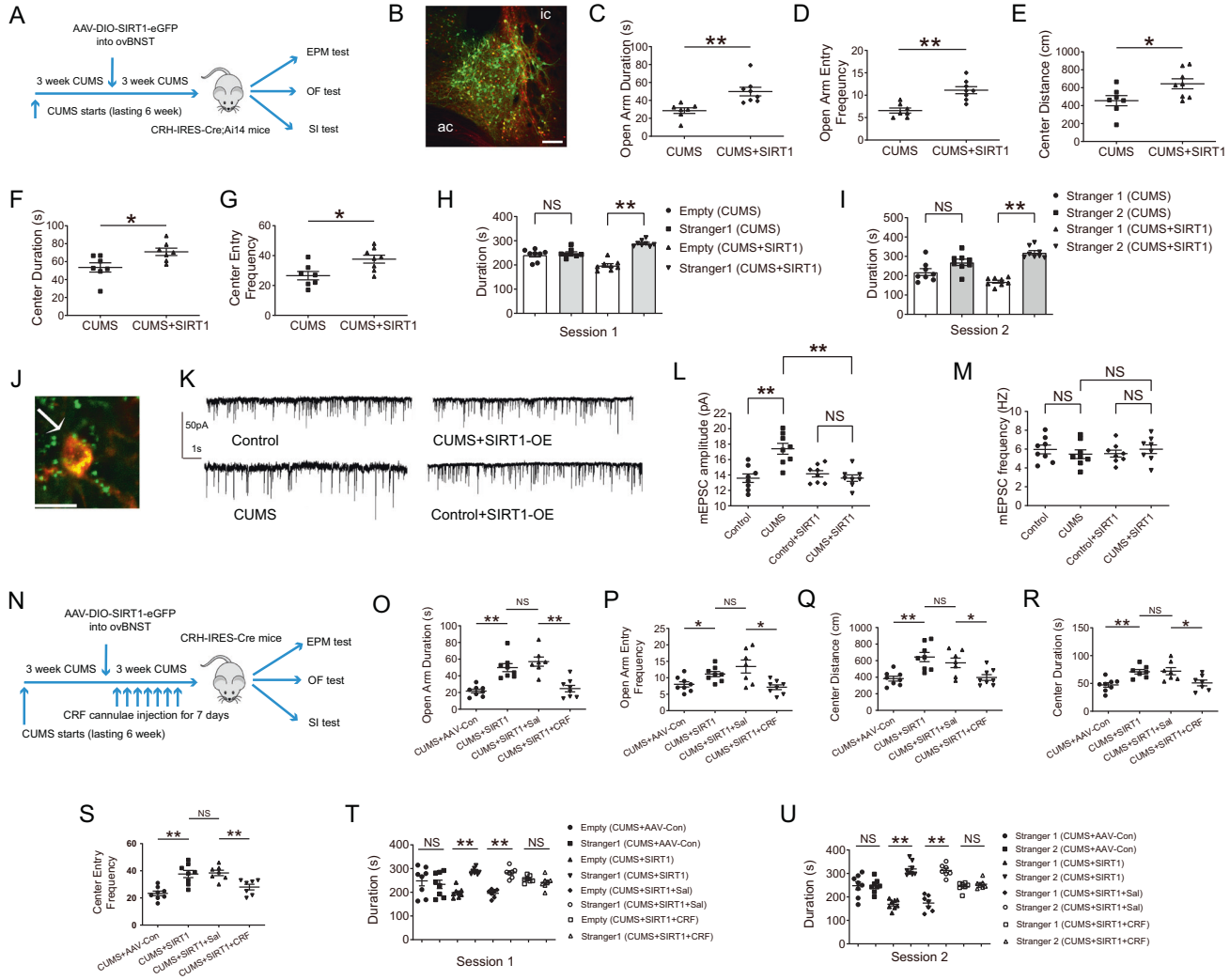


Fig. 3 Downregulation of CRF is required for the anxiolytic phenotype induced by SIRT1 overexpression. A Experimental schematics. AAV-DIO-SIRT1-eGFP was delivered to the ovBNST of *CRH-IRES-Cre;*Ai14 reporter mice at beginning of the fourth week during CUMS procedure. Anxiety-related behaviors were assessed after end of CUMS. **B** Fluorescence picture showing expression of AAV-DIO-SIRT1-eGFP (green) and CRF-tdTomato neurons (red) in the BNST of reporter mice. ic internal capsule, ac anterior commissure. Scale bar: 100 μm. **C**, **D** SIRT1-OE resulted in increased duration stay and entry frequency in EPM open arms for CUMS mice (both $p < 0.01$). $N = 7$-8 mice per group. **E**–**G** In the OF center, SIRT1-OE ($n = 7$-8) resulted in increased traveling distance, duration stay and entry frequency (all $p < 0.05$), as compared with CUMS mice ($n = 7$). **H**, **I** SIRT1-OE ($n = 8$) resulted in increased contact duration towards Stranger 1 mice vs. empty cage in SI test 1, and towards Stranger 2 mice vs. Stranger 1 mice in SI test 2 ($p < 0.01$ for both tests), as compared with CUMS mice ($n = 8$; in both tests $p > 0.05$). **J** *Post-hoc* confirmation of patched ovBNST CRF^{+} cell (red; pointed by white arrow), with Neurobiotin (green) penetrated through internal solution (merged in yellow; scale bar: 20 μm), recorded in BNST slices from reporter mice. **K** mEPSC trace example across non-stressed Control, CUMS, CUMS+SIRT1-OE and Control+SIRT1-OE mice. Scale bar: 50 pA and 1 s. **L**, **M** Comparison of mEPSC amplitude and frequency among the 4 groups. $N = 8$ cells per group. **N** Experimental schematics showing that during 6-week CUMS procedure, AAV-DIO-SIRT1-eGFP was delivered into ovBNST of *CRH-IRES*-Cre mice at the beginning of the 4th week. CRF was then infused into ovBNST for a continuous 7-day period through cannulae during the final week of CUMS. Anxiety-related behavioral tests were examined. **O**, **P** When CRF was infused for 7 days into SIRT1-OE mice subjected to CUMS (CUMS+SIRT1+CRF), compared with saline-infused group (CUMS+SIRT1+Sal), there was a significant decrease in the duration and entry frequency in EPM open arms. In contrast, SIRT1 overexpression in CUMS mice (CUMS+SIRT1) results in an increase in the duration and frequency in EPM open arms, as compared with control vector overexpression (CUMS+AAV-Con). ANOVA reveals a significant group difference for EPM open arm duration (**O**): $F(3,27) = 17.59$, $p < 0.001$; and for EPM open arm entry frequency (**P**): $F(3,27) = 6.469$, $p = 0.002$. $N = 7$-8 per group. **Q**–**S** Similarly, for CUMS mice overexpressing SIRT1 (SIRT1-OE), in the OF center, when CRF was infused for 7 days, compared with saline infusion, there was a significant decrease in the traveling distance, duration, or entry frequency between these 2 groups. In contrast, SIRT1 overexpression in CUMS mice results in an increase in the above parameters in the OF center, compared with control vector overexpression. ANOVA reveals a significant group difference for OF center distance (**Q**): $F(3,27) = 8.317$, $p < 0.001$; for center duration (**R**): $F(3,25) = 6.959$, $p = 0.002$; and for center entry frequency (**S**): $F(3,26) = 11.97$, $p < 0.001$. $N = 7$-8 per group. **T**–**U** When CRF was infused into BNST of SIRT1-overexpressed CUMS mice (CUMS+SIRT1+CRF group; $n = 7$), there was no difference in the contact duration towards Stranger 1 vs. empty cage in SI test 1, or towards Stranger 2 vs. Stranger 1 in SI test 2, which was similar to CUMS mice overexpressing control vector ($n = 8$; $p > 0.05$ in both SI test 1 and SI test 2). In contrast, for those CUMS mice overexpressing SIRT1 or those saline-infused CUMS mice overexpressing SIRT1, increased contact duration was found towards Stranger 1 vs. empty cage in SI test 1 (both $p < 0.01$), and towards Stranger 2 vs. Stranger 1 in SI test 2 (both $p < 0.01$). $^{**}p < 0.01$; $^{*}p < 0.05$; NS non-significant.

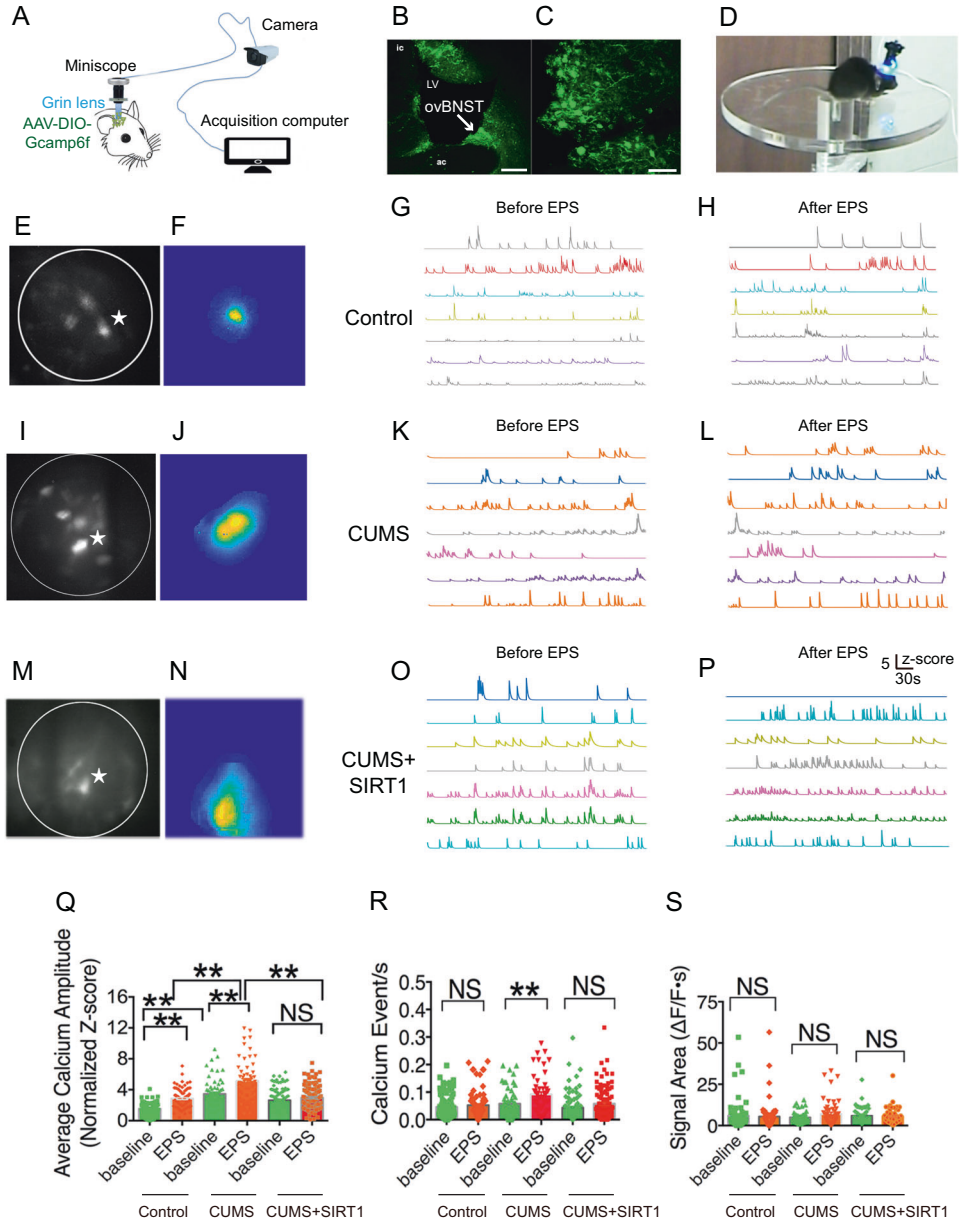
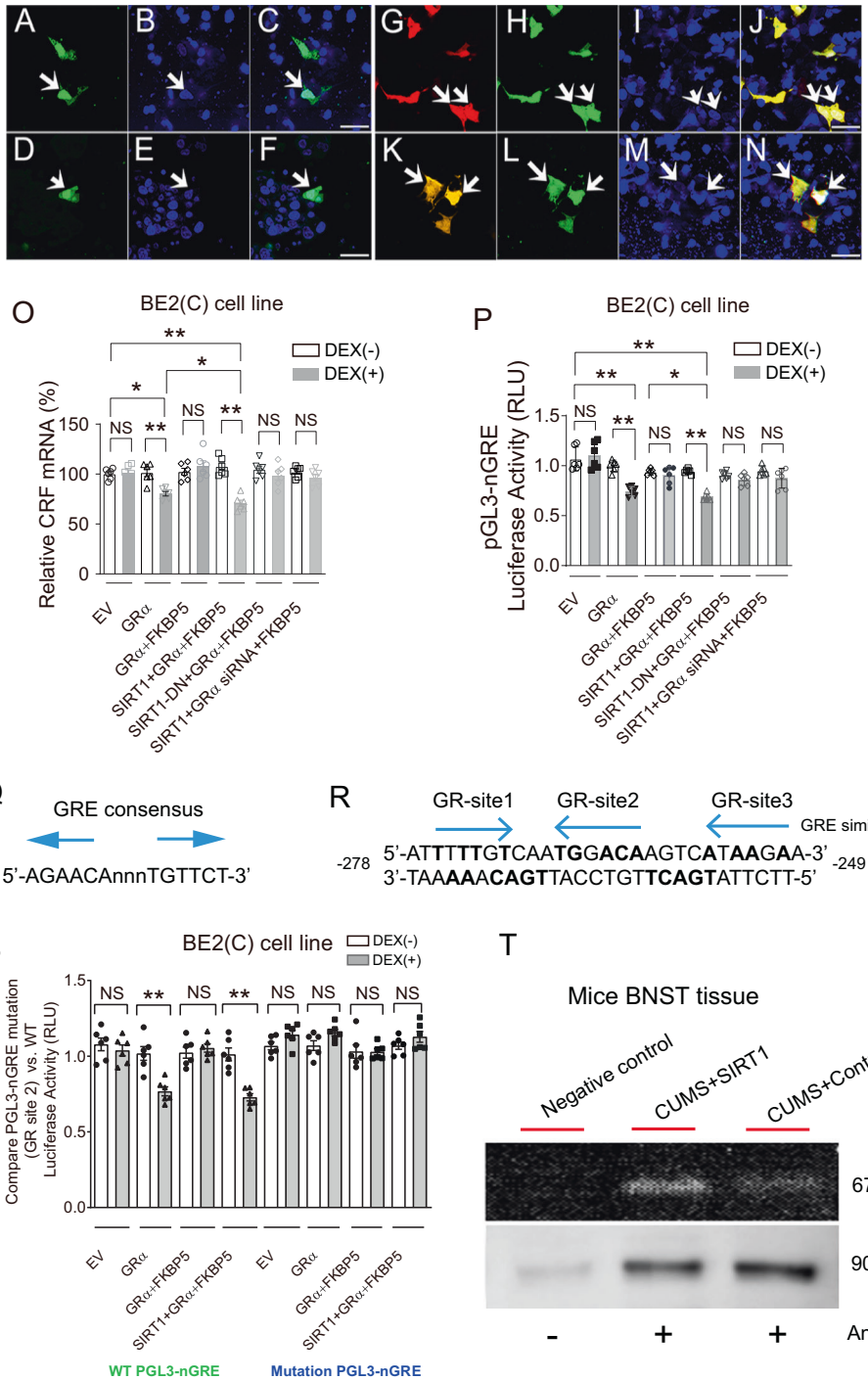


Fig. 4 SIRT1 overexpression normalizes the hyperactivity of CRF neurons in the BNST of chronically stressed mice, which are recruited during anxiogenic behaviors. A Example of in vivo MiniScope calcium imaging. A grin lens was mounted on mouse head and coupled to the camera connected to acquisition computer, which enables real-time monitoring of freely moving mice. **B** AAV-DIO-GCaMP6f fluorescence confirms the location of grin lens embedded into ovBNST of *CRH-IRES*-Cre mice. White arrow points to *post-hoc* confirmation of location of the tip of lens, which should be within the boundary of ovBNST. ic internal capsule, ac anterior commissure. Scale bar: 100 µm. **C** Amplified example of AAV-DIO-GCaMP6f fluorescence picture. Scale bar: 50 µm. **D** Schematics of elevated plus standing (EPS) paradigm, during which mice were put onto a 1.5 m high platform with the camera mounted on the head. A typical average calcium intensity image (**E**) under view from Control mouse; white star marks the recorded cell enlarged in (**F**). Representative example of recorded BNST CRF neuron from a Control mouse was shown. Representative calcium traces from a Control mouse (Z-score value plotted against time) at baseline (**G**; before EPS) and after EPS (**H**). Typical average calcium intensity image (**I**) under view from CUMS mouse; white star marks the recorded BNST CRF cell enlarged in **J**. Representative calcium traces from a CUMS mice at baseline (**K**) and after EPS (**L**). **M**, **N** Typical average calcium intensity image under view from a CUMS+SIRT1 mouse; the white star marks recorded BNST CRF cell enlarged in **N**. **O**, **P** Representative calcium traces from a CUMS +SIRT1 mice at baseline and after EPS. **Q** Normalized Ca^{2+} average amplitude (Z-score) before vs. after EPS, across the Control ($p < 0.01$), CUMS ($p < 0.01$), and CUMS+SIRT1 ($p > 0.05$) groups (all $n = 6$ mice). **R** Average calcium event frequency before vs. after EPS, compared across these 3 groups. Increased event frequency was found only in the CUMS group ($p < 0.01$). $N = 6$ mice per group. **S** Average signal area before vs. after EPS, compared across these 3 groups ($n = 6$ per group). No difference was found across the 3 groups after vs. before EPS (all $p > 0.05$). $^{**}p < 0.01$; NS non-significant. Scale bar: 30 s, Z-score = 5.

receptor (GR), to investigate how CRF downregulation is linked to SIRT1, we examined GR-mediated CRF transcriptional repression in vitro. The negative glucocorticoid response element (nGRE) on the human CRF promoter [38, 39] is located between nt −278 to −249, whose deletion resulted in complete loss of dexamethasone (DEX)-mediated CRF repression [13]. Hence, we used the hCRF promoter-based pGL3-nGRE luciferase reporter assay in the human BE(2)C cell line, which intrinsically produces CRF [40]. Given the importance of FKBP5 in regulating stress response and GR sensitivity, we also tested the effect of FKBP5.



First, SIRT1-GFP (Fig. 5A–C) or mutant SIRT1-DN-GFP (Fig. 5D–F) was transfected to examine its cellular localization. Next, SIRT1 was co-transfected with either GRα or FKBP5. Immunofluorescence revealed a clear co-localization of both SIRT1 (mCherry; red) with GRα (GFP; green) (Fig. 5G–J), and of SIRT1 (GFP; green) with FKBP5 (OFP; orange) (Fig. 5K–N).

Next, we examined the effects of transfecting different combinations of plasmids, with or without 24 h DEX treatment, on the CRF mRNA level (Fig. 5O). When we transfected GRα, we observed an effective transcriptional repression upon DEX as reflected by decreased CRF mRNA levels ($p = 0.004$). However, when co-transfected with FKBP5, the repressive effect of GRα was abolished ($p = 0.716$), confirming an inhibitory function of FKBP5. Interestingly, co-transfection of SIRT1 restored the transcriptional repression of GRα ($p = 0.002$). However, either knocking down GRα with siRNA ($p = 0.571$), or co-transfection with the enzyme-deficient SIRT1-DN ($p = 0.802$), had no effect.

We further performed a pGL3-nGRE luciferase activity assay (Fig. 5P) to test transcriptional activity changes, using the same conditions described above (see Fig. 5O). Similar results were found, as GRα's function was again restored following co-transfection of SIRT1 ($p = 0.002$). Knocking down Grα ($p = 0.240$) or co-transfecting enzyme-deficient SIRT1-DN ($p = 0.310$) had no effect.

The GRE consensus site (sense strand) that supports GR-dimer binding is shown in Fig. 5Q [41]. Within nt −278 and −249, 3 sites

Fig. 5 SIRT1 enhances GRα-mediated transcriptional repression of CRF. A–C Co-localization pattern of SIRT1-eGFP (green) and DAPI (blue) in the human neuroblastoma BE2C cells. Scale bar: 50 µm. **D–F** Co-localization pattern of mutant SIRT1-DN-eGFP (green) and DAPI (blue). Scale bar: 50 µm. Co-localization pattern (**J**; yellow) of SIRT1-mCherry (**G**; red) and GRα-GFP (**H**; green) with DAPI (**I**; blue). Scale bar: 50 µm. Co-localization pattern (**N**; cyan) of FKBP5-OFP (**K**; orange) and SIRT1-GFP (**L**; green) with DAPI (**M**; blue). Scale bar: 50 µm. **O** BE2C cells were transfected with different combinations of plasmids. qPCR assays were performed to compare *CRF* mRNA expression before vs. after dexamethasone (DEX) treatment, for the following conditions: 1) empty vehicle (EV) ($p > 0.05$), 2) GRα ($p < 0.01$), 3) GRα + FKBP5 ($p > 0.05$), 4) SIRT1+GRα+FKBP5 ($p < 0.01$), 5) SIRT1-DN+GRα+FKBP5 ($p = 0.802$), and 6) SIRT1+GRα-siRNA+FKBP5 ($p > 0.05$). $N = 6$ wells for each condition group. **P** Luciferase activity assay, with pGL3-nGRE luciferase reporter construct targeting 1×nGRE sequence located at −278 to −249 nt on human CRF promoter, was performed to examine the transcriptional activity at human CRF promoter before vs. after DEX treatment, under the same transfection conditions as described in **O**. $N = 6$ wells for each condition group. **Q** Sites of GRE half-site consensus sequence at human CRF locus promoter region, as reported in literature [39]. **R** Three consensus 6-bp GR binding sites are shown at the hCRF promoter region, including GR-site 1, GR-site 2, and GR-site3 [39], as reported in literature. For the mutants, the site-2 was mutated into *Eco*RI restriction sites (5′-GAATTC-3′) [39]. **S** Comparison of pGL3-nGRE-luciferase reporter activity with vs. without DEX treatment after mutation of GR-binding site 2 under different transfection conditions, including: 1) the empty vehicle (EV) group ($p > 0.05$), 2) GRα group ($p > 0.05$), 3) GRα together with FKBP5 group ($p > 0.05$), and 4) the SIRT1+GRα+FKBP5 group ($p > 0.05$). By contrast, for wild-type (WT) nGRE promoter, DEX incubation results in a decrease in Luciferase activity in both GRα group ($p < 0.05$) and SIRT1+GRα+FKBP5 group ($p < 0.05$). $N = 6$ wells for each condition group. **T** BNST tissue from SIRT1-overexpressed CUMS mice vs. Control vector-overexpressed CUMS mice were subjected to chromatin immunoprecipitation (ChIP) with an anti-GRα antibody, followed by qPCR for the nGRE sequence on *CRF* promoter. Top picture shows representative PCR bands example of GR-antibody-bound DNA regions; bottom picture shows corresponding GR western blot bands (molecular weight around 90 kDa) from each group respectively. For the negative control group, the tissue was processed without pre-incubation with GR-antibody. $^{**}p < 0.01$; $^{*}p < 0.05$; NS non-significant.

(sites 1-3) contain a half-site homology; among these, the site 2 conferred the highest GR DNA-binding domain (DBD) affinity [41] (Fig. 5R). We therefore mutated GR-binding site 2 and performed another luciferase assay.

As shown in Fig. 5S, as compared with transfection with un-mutated wildtype (WT) PGL3-nGRE, for both GRα group and co-transfection of SIRT1 with GRα and FKBP5 group, a significant decrease in Luciferase activity was observed when DEX was applied to cells (*p* value: empty vehicle (EV) group: $p = 0.485$; GRα group: $p = 0.004$; GRα + FKBP5 group: $p = 0.488$; SIRT1+GRα +FKBP5 group: $p = 0.002$). However, when we transfected nGRE containing the binding site-2 mutation, upon GRα transfection, surprisingly, there was no difference in Luciferase activity upon application of DEX to cells ($p = 0.053$). Also, co-transfection of GRα and SIRT1 together with FKBP5, yielded no difference upon DEX ($p = 0.057$), indicating that SIRT1's normalizing effect was dependent on intact GR binding. Co-localization pattern of SIRT1 with either GR or FKBP5 in the mouse BNST was confirmed by IHC (shown in Supplementary Fig. S11).

We next extracted BNST tissue and performed chromatin immunoprecipitation (ChIP) followed by a qPCR assay. Interestingly, an increase was found in the amount of PCR bands of DNA bound to GR-antibody at the nGRE of CRF promoter from SIRT1-OE CUMS mice, as compared to those from CUMS mice over-expressing control-vector (Fig. 5T). Together, SIRT1 overexpression enhances GR binding to the CRF promoter and thus strengthens GR-mediated CRF transcriptional repression.

SIRT1 deacetylates FKBP5 to facilitate its dissociation from the GR

Since FKBP5 can sequester the GR to restrict its function and inhibit transcription [25, 42], we hypothesized that SIRT1 may directly regulate the interaction between FKBP5 and GRα. We examined: (1) possible interactions between these three proteins; (2) possible effect of SIRT1 on FKBP5-GR binding.

Prior to immunoprecipitation (IP), we transiently expressed plasmids containing; 1) HA-tagged SIRT1 and FKBP5; 2) His-tagged FKBP5 and SIRT1 or GRα; or 3) Flag-tagged GRα and FKBP5, into HEK293T cells. Interestingly, SIRT1 directly interacted with FKBP5 (Fig. 6A) and vice versa, FKBP5 also reciprocally interacted with SIRT1 (Fig. 6B).

We next examined FKBP5-GR interaction. Consistent with prior literature [25], GRα and FKBP5 were found to reciprocally interact with each other (Fig. 6C, D). We next co-transfected SIRT1 and again compared the interaction between GRα and FKBP5. Notably, the binding between these two proteins was diminished by HA-SIRT1 (Fig. 6E), which was in contrast to co-treatment with the SIRT1 antagonist EX527. In contrast, SIRT1 depletion increased binding between GRα and FKBP5, as found after SIRT1-siRNA treatment (Fig. 6E). These data indicate that SIRT1 facilitates FKBP5 dissociation from GRα.

Since SIRT1 acts through deacetylation [43], we examined FKBP5 acetylation status. HEK293 cells were transfected with His-FKBP5 paired with different plasmid condition. FKBP5 acetylation was then examined by IP with anti-FKBP5 followed by IB with acetylated lysine (ac-K) antibody. WT-SIRT1 (but not SIRT1-DN) decreased FKBP5 acetylation, while SIRT1 depletion led to an increased acetylation (Fig. 6F). Similar results were found for reciprocal pull-downs of FKBP5 by IP with ac-K antibody (Fig. 6G). Collectively, SIRT1 directly interacts with FKBP5 and promotes its deacetylation.

Acetylation is regulated by opposing actions of acetyltransferases and deacetylases. To identify possible acetyltransferases, we transfected cells with either HA-SIRT1 or established acetyltransferase, p300 (EP300) or CBP (CREB-binding protein). Both have been reported to regulate FKBP5 acetylation status [44, 45]. Compared to EV or SIRT1, HA-CBP resulted in a significant increase in ac-K level, whereas HA-p300 resulted in a slightly lower increase (Fig. 6H). Therefore, CBP was identified as the main acetyltransferase partner with SIRT1. Furthermore, a reciprocal interaction between FKBP5 and CBP was revealed (Fig. 6I), further supporting the direct interactions between them.

Having determined that FKBP5 is indeed deacetylated by SIRT1, we next analyzed possible acetylation sites targeted by SIRT1, by using mass spectrometry (MS) in HEK293T cells, under either SIRT1-depletion or control conditions. As shown in Fig. 6J, we detected 6 lysine residues (264, 397, 208, 342, 432, and 65) on FKBP5 that demonstrated different acetylation level upon SIRT1 depletion. To identify the exact lysine residues regulated by SIRT1, we performed site-directed mutagenesis (Fig. 6K). Lysine (K) was mutated into arginine (R) to mimic the non-acetylated form. Cells were transfected with indicated constructs of His-FKBP5, with or without SIRT1-siRNAs. Acetylation of FKBP5 was examined with an antibody for ac-K after IP with His. As shown in Fig. 6K, SIRT1 depletion increased the acetylation of WT FKBP5, which was blunted with K264R, K342R, and K65R single mutants, indicating these three lysine sites could be the main targeted acetylation sites.

Next, we mutated all these three lysine residues simultaneously (3KR) and expressed this 3KR-mutant in HEK293T cells (Fig. 6L). Knocking down SIRT1 increased acetylation for WT FKBP5, but not for this 3KR mutant, confirming that K264, K342, and K65 are the major acetylation sites targeted by SIRT1. Therefore, SIRT1

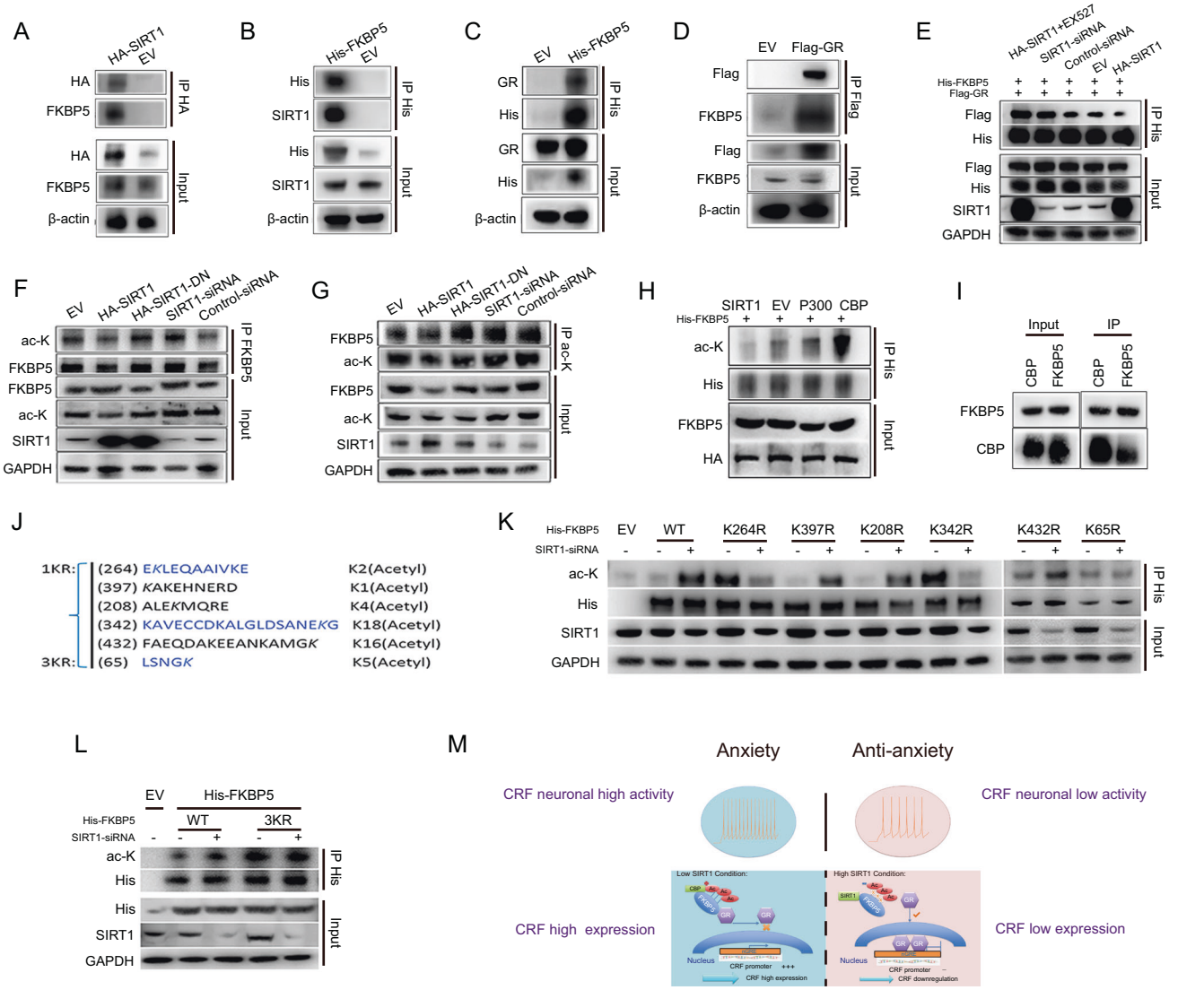


Fig. 6 SIRT1 promotes FKBP5 deacetylation to facilitate its dissociation from GR. A In HEK293T cells, immunoprecipitation (IP) data shows that HA-SIRT1 interacts with His-FKBP5. **B** His-FKBP5 reciprocally interacts with HA-SIRT1. **C** IP data shows His-FKBP5 could also interact with Flag-GR. **D** Flag-GR can reciprocally interact with His-FKBP5. **E** When full-length HA-SIRT1 was co-transfected with Flag-GR, the interaction of GR and FKBP5 was decreased compared with empty vehicle Control (EV) condition; whereas knocking down SIRT1 with siRNA increased the FKBP5-GR interaction, similar to co-treatment with SIRT1-selective antagonist EX527. **F** HEK293T cells were transfected with either empty vehicle (EV), full-length HA-SIRT1, mutant HA-SIRT1-DN, SIRT1-siRNA or Control-siRNA, together with His-FKBP5. Lysine acetylation on FKBP5 was detected by immunoblot (IB) with an ac-K (acetylated lysine) antibody after IP with FKBP5 antibody. **G** HEK293T cells were co-transfected with the same plasmid conditions as in **F**. Acetylation status of FKBP5 was examined with IB using FKBP5 antibody after IP with ac-K antibody. **H** HEK293T cells were co-transfected with His-FKBP5 combined with different plasmids encoding either: 1) full-length HA-SIRT1, or 2) empty vehicle (EV), or 3) P300 or 4) CBP. Acetylation of FKBP5 was then examined with IB using ac-K antibody after IP with His antibody. **I** Reciprocal IP assay between CBP and FKBP5. **J** A list of acetylation sites in FKBP5 protein analyzed by mass spectrometry (MS). **K** HEK293T cells were transfected with or without SIRT1-siRNA, combined with indicated wild-type (WT) or each single-site mutant FKBP5 form. Lysine (K) was mutated into arginine (R) to mimic non-acetylated form. After 48 h, acetylation of FKBP5 was examined by pull-down with anti-His antibody followed by western blot with ac-K antibody. **L** HEK293 cells were transfected with indicated wild-type (WT) FKBP5 or 3-mutant constructs (3KR) with or without SIRT1-siRNA. Acetylation of FKBP5 was examined by pull-down with anti-His antibody followed by western blot for ac-K. **M** A cell model illustrating that both lower CRF neuronal activity and decreased CRF expression contribute to the anxiolytic effects of SIRT1. The upper pictures illustrate higher CRF neuronal activity under CUMS condition (left), compared with lower CRF neuronal activity under SIRT1-overexpression condition (right). The bottom pictures illustrate the different interaction among FKBP5, GR and SIRT1, resulting in differential CRF transcription. Under low SIRT1 condition (left), increased acetylation of FKBP5 by CBP promotes its binding with GR, thereby sequestering and preventing GR entry into nucleus. This results in more CRF production. Upon SIRT1 activation or overexpression condition (right), deacetylation of FKBP5 promotes its dissociation from GR, effectively de-repressing GR entry into the nucleus. Finally, enhanced GR binding on the nGRE sequence of CRF promoter will amplify its transcriptional repression function and promote CRF downregulation.

regulates acetylation of FKBP5 mainly at lysine 264, 342 and 65 sites.

A cellular model, illustrating parallel mechanisms (both CRF neuronal activity change and CRF transcription level change) may contribute to the anxiolytic effects of SIRT1, is shown in Fig. 6M. The differential expression of CRF is achieved by differential GR transcriptional status, mediated via different acetylation status of FKBP5.

To further explore how CUMS or SIRT1 overexpression affects FKBP5 protein expression level, we extracted BNST tissue and

compared FKBP5 protein expression levels among different groups (Supplementary Fig. S12). The results show that no significant effect of SIRT1 on FKBP5 protein expression was found, indicating that the anxiolytic effects of SIRT1 are mainly attributed to its acetyl regulation of FKBP5.

DISCUSSION

SIRT1 has been extensively implicated in mood disorders [7, 9–11]. Although the BNST serves as a key limbic 'hub' region involved in the control of anxiety responses, the exact role of SIRT1 within the BNST in regulating anxiety remained unclear. Using region- and cell-type- specific manipulations, we found SIRT1 overexpression in the ovBNST reverses chronic stress-induced anxiety-like phenotype, mediated via CRF downregulation. This is the first study linking SIRT1, a deacetylase, to CRF, a key stress neuropeptide [46, 47]. Indeed, SIRT1 expression in the BNST was compromised by CUMS, whereas knocking down SIRT1 in stress-free (naïve) mice conversely produced an anxiogenic phenotype (Supplementary Fig. S9), confirming its tonic anxiolytic role in the BNST. Particularly, SIRT1 expression intensity is shown to be decreased in those BNST CRF-positive cells under CUMS condition (Fig. 1U, V). Since CRF in the BNST mediates stress-induced anxiety [18], CRF downregulation plays a central role here (Fig. 3N–U). Further molecular analysis revealed that deacetylation of FKBP5 facilitates its dissociation from the GR, which enhances CRF transcriptional repression. Overall, these findings highlight a so far unrecognized, CRF-dependent mechanism underlying the anxiolytic role of SIRT1 via deacetylation of FKBP5.

Recent report shows selective upregulation of FKBP5 in the paraventricular nucleus CRH neurons after acute stress, whereas overexpression of FKBP5 results in HPA hyper-activation [48]. Despite the importance of FKBP5 in stress biology [23, 49] and its interactions with stress hormone receptors [25, 50], a detailed functional regulation of FKBP5 by SIRT1 has been rarely explored. Our in vitro data reveal that SIRT1 deacetylates FKBP5 and thereby strengthens the GR-mediated CRF transcriptional repression, as confirmed by ChIP assay data in vivo (Fig. 5T). Still, to exactly decipher the processes in vivo, further in-depth investigation may be needed. Also, while SIRT1 regulates the acetylation of various transcription factors and enzymes [51], deacetylation of FKBP5 by SIRT1 did not alter its transcription. Rather, such regulation may modulate other functions of FKBP5, e.g. its interaction with other transcriptional factors (here e.g. the GR). We therefore propose that deacetylation may yield a conformational change, that will be required for the dissociation of FKBP5 from the GR, which will ultimately enhance GR binding at CRF promoters.

As anxiety disorders are complex [52, 53], regulation of CRF expression may obviously not be the exclusive mechanism underlying its etiology. Further details regarding e.g. the dynamics of GR-transcription in this respect await future study. Also, our MiniScope calcium imaging data demonstrate a decreased neuronal activity of CRF cells after SIRT1 overexpression, pointing to a parallel regulatory mechanism (Fig. 6M). Under chronic stress condition, CRF neurons display a high activity; this was accompanied by a high level of CRF transcription and expression, resulting in anxiety phenotype. Upon high SIRT1 condition, lower activity of CRF neurons accompanied by CRF downregulation ensures an anxiolytic phenotype. Although whether and how CRF neuronal activity changes may result in transcriptional change of CRF mRNA level remains unknown, one recent study reported that during chronic morphine withdrawal, optogenetically inhibiting parvalbumin (PV) interneurons in the central amygdala attenuated elevated CRF mRNA level [54]. In addition, literature have reported that BNST CRF cells could project onto ventral tegmental area [55], hypothalamic periventricular nucleus [56], lateral hypothalamus [57], etc, all of which belong to key stress-responsive regions. Therefore, these projections may also contribute to stress-related anxiety disorders; although whether SIRT1 may also potentially affect these projections, and whether SIRT's effects on these CRF projections may further contribute to its anxiolytic effects deserve future investigations.

Our study shows that around 70% CRF cells co-localize with the inhibitory transmitter GABA within the ovBNST (Supplementary Fig. S13), which is in line with previous literature [58], showing that CRF cells co-localize more with GABA in the dorsal BNST. Furthermore, our retro-tracing study shows that RV-labeled CRHR1 cells could retro-trace onto local CRF cells within the ovBNST (Supplementary Fig. S13), indicating existence of a local micro-circuit projection from CRF cells to CRHR1 cells. Future studies will be needed to further elucidate the role of this micro-circuitry in the stress-induced mood regulation. Moreover, many anxiety-related disorders are also characterized by a disruption in social behavior, which is why we here applied social interaction (SI) tests [30] to examine social anxiety as well. Indeed, CUMS mice displayed a typical social anxiety phenotype, which was restored by SIRT1 overexpression, confirming that the anxiolytic effects of SIRT1 at least involve multiple anxiety domains.

Importantly, our data further report an increased expression of CRF in the BNST of stressed mice (Fig. 1M–O). Given that CRF mRNA level is upregulated (Fig. 1P), this pointed to an increase in CRF transcription and expression, reflected by increased numbers of neurons expressing CRF (Fig. 1O). An alternative explanation, i.e. an increase in (new) CRF cells, was excluded, as the BNST is not a neurogenic region. In addition to the BNST, CRF is also highly expressed in other brain regions, including the amygdala (basolateral amygdale [59] and central amygdale [60, 61]), hippocampus [62], hypothalamus [63], etc, and CRF in these regions is involved in anxiety regulation (see references above). All these, often interconnected, regions also play an important role in stress regulation. Here, we focused on the BNST, and showed that by manipulating SIRT1 in the BNST, chronic stress-induced anxious behaviors could be rescued, highlighting the BNST as an important key hub region in anxiety regulation. Still, future studies should also address the role of these other brain regions.

In this study, no significant effect of SIRT1 on FKBP5 protein expression was observed (Supplementary Fig. S12). We therefore assume that the anxiolytic effects of SIRT1 are largely attributed to its acetyl regulation of FKBP5. Also, consistent with the notion that stress induces hyper-activation of the CRF neurons in the BNST [64, 65], our MiniScope real-time calcium imaging data revealed potentiated calcium responses upon EPS in CUMS-exposed mice, which were reversed by SIRT1-OE. These data provide direct in vivo evidence for an anxiolytic role of SIRT1.

There are also some limitations to our study. First, for simplicity, all animals we used were male. Given that BNST is a sexually-dimorphic region [66], future studies should also explore these effects in female mice. Second, future research may also need to explore the deacetylation details in the BNST in vivo.

Taken together, we here demonstrate an anxiolytic role for SIRT1 signaling in the mouse BNST, which is mediated by CRF downregulation and lower CRF neuronal activity (graphical cartoon shown in Supplementary Fig. S14). We further show that CRF downregulation is mediated at least in part, by enhanced glucocorticoid receptor (GR)-mediated CRF transcriptional repression through deacetylation of FKBP5. These findings will broaden our understanding of the role of SIRT1 in anxiety disorders and raise the possibility to develop future therapeutic strategies towards targeting SIRT1 signaling to treat stress-related anxiety disorders.

Study approval

The animal studies conducted in the work were approved by the Institutional Animal Care and Use Committees of University of Science and Technology of China (Life Science School, USTC, Hefei, China).

REFERENCES

1. Kessler RC, Berglund P, Demler O, Jin R, Merikangas KR, Walters EE. Lifetime prevalence and age-of-onset distributions of DSM-IV disorders in the National Comorbidity Survey Replication. Arch Gen Psychiatry. 2005;62:593–602.
2. Joels M, Baram TZ. The neuro-symphony of stress. Nat Rev Neurosci. 2009;10:459–66.
3. Lucassen PJ, Pruessner J, Sousa N, Almeida OF, Van Dam AM, Rajkowska G, et al. Neuropathology of stress. Acta Neuropathol. 2014;127:109–35.
4. Gao J, Wang WY, Mao YW, Graff J, Guan JS, Pan L, et al. A novel pathway regulates memory and plasticity via SIRT1 and miR-134. Nature. 2010;466:1105–9.
5. Michan S, Li Y, Chou MM, Parrella E, Ge H, Long JM, et al. SIRT1 is essential for normal cognitive function and synaptic plasticity. J Neurosci. 2010;30:9695–707.
6. Herskovits AZ, Guarente L. SIRT1 in neurodevelopment and brain senescence. Neuron. 2014;81:471–83.
7. Kim HD, Hesterman J, Call T, Magazu S, Keeley E, Armenta K, et al. SIRT1 mediates depression-like behaviors in the nucleus accumbens. J Neurosci. 2016;36:8441–52.
8. Abe-Higuchi N, Uchida S, Yamagata H, Higuchi F, Hobara T, Hara K, et al. Hippocampal sirtuin 1 signaling mediates depression-like behavior. Biol Psychiatry. 2016;80:815–26.
9. Lei Y, Wang J, Wang D, Li C, Liu B, Fang X, et al. SIRT1 in forebrain excitatory neurons produces sexually dimorphic effects on depression-related behaviors and modulates neuronal excitability and synaptic transmission in the medial prefrontal cortex. Mol Psychiatry. 2020;25:1094–111.
10. Yu D, Homiack DR, Sawyer EJ, Schrader LA. BK channel deacetylation by SIRT1 in dentate gyrus regulates anxiety and response to stress. Commun Biol. 2018;1:82–95.
11. Libert S, Pointer K, Bell EL, Das A, Cohen DE, Asara JM, et al. SIRT1 activates MAO-A in the brain to mediate anxiety and exploratory drive. Cell. 2011;147:1459–72.
12. Zhou C, Wu Y, Ding X, Shi N, Cai Y, Pan ZZ. SIRT1 decreases emotional pain vulnerability with associated CaMKIIalpha deacetylation in central amygdala. J Neurosci. 2020;40:2332–42.
13. Marcinkiewcz CA, Mazzone CM, D'Agostino G, Halladay LR, Hardaway JA, DiBerto JF, et al. Serotonin engages an anxiety and fear-promoting circuit in the extended amygdala. Nature. 2016;537:97–101.
14. Choi DC, Furay AR, Evanson NK, Ostrander MM, Ulrich-Lai YM, Herman JP. Bed nucleus of the stria terminalis subregions differentially regulate hypothalamic-pituitary-adrenal axis activity: implications for the integration of limbic inputs. J Neurosci. 2007;27:2025–34.
15. Duvarci S, Bauer EP, Pare D. The bed nucleus of the stria terminalis mediates inter-individual variations in anxiety and fear. J Neurosci. 2009;29:10357–61.
16. Kim SY, Adhikari A, Lee SY, Marshel JH, Kim CK, Mallory CS, et al. Diverging neural pathways assemble a behavioural state from separable features in anxiety. Nature. 2013;496:219–23.
17. Henckens M, Printz Y, Shamgar U, Dine J, Lebow M, Drori Y, et al. CRF receptor type 2 neurons in the posterior bed nucleus of the stria terminalis critically contribute to stress recovery. Mol Psychiatry. 2017;22:1691–1700.
18. Hu P, Liu J, Maita I, Kwok C, Gu E, Gergues MM, et al. Chronic stress induces maladaptive behaviors by activating corticotropin-releasing hormone signaling in the mouse oval bed nucleus of the stria terminalis. J Neurosci. 2020;40:2519–37.
19. Willner P. The chronic mild stress (CMS) model of depression: history, evaluation and usage. Neurobiol Stress. 2017;6:78–93.
20. Daniel SE, Rainnie DG. Stress modulation of opposing circuits in the bed nucleus of the stria terminalis. Neuropsychopharmacology. 2016;41:103–25.
21. Muglia LJ, Jacobson L, Luedke C, Vogt SK, Schaefer ML, Dikkes P, et al. Corticotropin-releasing hormone links pituitary adrenocorticotropin gene expression and release during adrenal insufficiency. J Clin Invest. 2000;105:1269–77.
22. Young CE, Tong Q. Corticotropin releasing hormone signaling in the bed nuclei of the stria terminalis as a link to maladaptive behaviors. Front Neurosci. 2021;15:642379.
23. Binder EB. The role of FKBP5, a co-chaperone of the glucocorticoid receptor in the pathogenesis and therapy of affective and anxiety disorders. Psychoneuroendocrinology. 2009;34:S186–195.
24. Touma C, Gassen NC, Herrmann L, Cheung-Flynn J, Bull DR, Ionescu IA, et al. FK506 binding protein 5 shapes stress responsiveness: modulation of neuroendocrine reactivity and coping behavior. Biol Psychiatry. 2011;70:928–36.
25. Li H, Su P, Lai TK, Jiang A, Liu J, Zhai D, et al. The glucocorticoid receptor-FKBP51 complex contributes to fear conditioning and posttraumatic stress disorder. J Clin Invest. 2020;130:877–89.
26. Hausl AS, Balsevich G, Gassen NC, Schmidt MV. Focus on FKBP51: a molecular link between stress and metabolic disorders. Mol Metab. 2019;29:170–81.
27. Hu P, Maita I, Phan ML, Gu E, Kwok C, Dieterich A, et al. Early-life stress alters affective behaviors in adult mice through persistent activation of CRH-BDNF signaling in the oval bed nucleus of the stria terminalis. Transl Psychiatry. 2020;10:396.
28. Samuels BA, Anacker C, Hu A, Levinstein MR, Pickenhagen A, Tsetsenis T, et al. 5-HT1A receptors on mature dentate gyrus granule cells are critical for the antidepressant response. Nat Neurosci. 2015;18:1606–16.
29. File SE, Seth P. A review of 25 years of the social interaction test. Eur J Pharm. 2003;463:35–53.
30. Kaidanovich-Beilin O, Lipina T, Vukobradovic I, Roder J, Woodgett JR. Assessment of social interaction behaviors. J Vis Exp. 2011;25:2473.
31. Qi XR, Zhao J, Liu J, Fang H, Swaab DF, Zhou JN. Abnormal retinoid and TrkB signaling in the prefrontal cortex in mood disorders. Cereb Cortex. 2015;25:75–83.
32. Hu P, Liu J, Zhao J, Qi XR, Qi CC, Lucassen PJ, et al. All-trans retinoic acid-induced hypothalamus-pituitary-adrenal hyperactivity involves glucocorticoid receptor dysregulation. Transl Psychiatry. 2013;3:e336.
33. Liang B, Zhang L, Barbera G, Fang W, Zhang J, Chen X, et al. Distinct and dynamic ON and OFF neural ensembles in the prefrontal cortex code social exploration. Neuron 2018;100:700–14 e709.
34. Chen P, Lou S, Huang ZH, Wang Z, Shan QH, Wang Y, et al. Prefrontal cortex corticotropin-releasing factor neurons control behavioral style selection under challenging situations. Neuron 2020;106:301–15 e307.
35. Zhang X, Lei B, Yuan Y, Zhang L, Hu L, Jin S, et al. Brain control of humoral immune responses amenable to behavioural modulation. Nature. 2020;581:204–8.
36. Zhou P, Resendez SL, Rodriguez-Romaguera J, Jimenez JC, Neufeld SQ, Giovannucci A, et al. Efficient and accurate extraction of in vivo calcium signals from microendoscopic video data. Elife. 2018;7:1–37.
37. Berton O, McClung CA, Dileone RJ, Krishnan V, Renthal W, Russo SJ, et al. Essential role of BDNF in the mesolimbic dopamine pathway in social defeat stress. Science. 2006;311:864–8.
38. Herman JP, Schafer MK, Thompson RC, Watson SJ. Rapid regulation of corticotropin-releasing hormone gene transcription in vivo. Mol Endocrinol. 1992;6:1061–9.
39. van der Laan S, de Kloet ER, Meijer OC. Timing is critical for effective glucocorticoid receptor mediated repression of the cAMP-induced CRH gene. PLoS One. 2009;4:e4327.
40. Yamamori E, Iwasaki Y, Taguchi T, Nishiyama M, Yoshida M, Asai M, et al. Molecular mechanisms for corticotropin-releasing hormone gene repression by glucocorticoid in BE(2)C neuronal cell line. Mol Cell Endocrinol. 2007;264:142–8.
41. Malkoski SP, Dorin RI. Composite glucocorticoid regulation at a functionally defined negative glucocorticoid response element of the human corticotropin-releasing hormone gene. Mol Endocrinol. 1999;13:1629–44.
42. Scammell JG, Denny WB, Valentine DL, Smith DF. Overexpression of the FK506-binding immunophilin FKBP51 is the common cause of glucocorticoid resistance in three New World primates. Gen Comp Endocrinol. 2001;124:152–65.
43. Liu T, Lin YH, Leng W, Jung SY, Zhang H, Deng M, et al. A divergent role of the SIRT1-TopBP1 axis in regulating metabolic checkpoint and DNA damage checkpoint. Mol Cell. 2014;56:681–95.
44. Yu J, Qin B, Wu F, Qin S, Nowsheen S, Shan S, et al. Regulation of serine-threonine kinase akt activation by NAD(+)-dependent deacetylase SIRT7. Cell Rep. 2017;18:1229–40.
45. Yang XJ. The diverse superfamily of lysine acetyltransferases and their roles in leukemia and other diseases. Nucleic Acids Res. 2004;32:959–76.
46. Lv Y, Chen P, Shan QH, Qin XY, Qi XH, Zhou JN. Regulation of cued fear expression via corticotropin-releasing-factor neurons in the ventral anteromedial thalamic nucleus. Neurosci Bull. 2021;37:217–28.
47. Wang T, Ma YN, Zhang CC, Liu X, Sun YX, Wang HL, et al. The nucleus accumbens CRH-CRHR1 system mediates early-life stress-induced sleep disturbance and dendritic atrophy in the adult mouse. Neurosci Bull. 2023;39:41–56.
48. Hausl AS, Brix LM, Hartmann J, Pohlmann ML, Lopez JP, Menegaz D, et al. The co-chaperone Fkbp5 shapes the acute stress response in the paraventricular nucleus of the hypothalamus of male mice. Mol Psychiatry. 2021;26:3060–76.
49. Engelhardt C, Tang F, Elkhateib R, Bordes J, Brix LM, van Doeselaar L, et al. FKBP51 in the oval bed nucleus of the stria terminalis regulates anxiety-like behavior. eNeuro. 2021;8:0425–0421.
50. Hartmann J, Bajaj T, Klengel C, Chatzinakos C, Ebert T, Dedic N, et al. Mineralocorticoid receptors dampen glucocorticoid receptor sensitivity to stress via regulation of FKBP5. Cell Rep. 2021;35:109185.
51. Haigis MC, Sinclair DA. Mammalian sirtuins: biological insights and disease relevance. Annu Rev Pathol. 2010;5:253–95.
52. Jimenez JC, Su K, Goldberg AR, Luna VM, Biane JS, Ordek G, et al. Anxiety cells in a hippocampal-hypothalamic circuit. Neuron. 2018;97:670–83 e676.
53. Leonardo ED, Hen R. Genetics of affective and anxiety disorders. Annu Rev Psychol. 2006;57:117–37.
54. Wang L, Shen M, Jiang C, Ma L, Wang F. Parvalbumin interneurons of central amygdala regulate the negative affective states and the expression of

corticotrophin-releasing hormone during morphine withdrawal. Int J Neuropsychopharmacol. 2016;19:pyw060.
55. Soden ME, Yee JX, Cuevas B, Rastani A, Elum J, Zweifel LS. Distinct encoding of reward and aversion by peptidergic BNST inputs to the VTA. Front Neural Circuits. 2022;16:918839.
56. Dabrowska J, Martinon D, Moaddab M, Rainnie DG. Targeting corticotropin-releasing factor projections from the oval nucleus of the bed nucleus of the stria terminalis using cell-type specific neuronal tracing studies in mouse and rat brain. J Neuroendocrinol. 2016;28. https://doi.org/10.1111/jne.12442.
57. Giardino WJ, Eban-Rothschild A, Christoffel DJ, Li SB, Malenka RC, de Lecea L. Parallel circuits from the bed nuclei of stria terminalis to the lateral hypothalamus drive opposing emotional states. Nat Neurosci. 2018;21:1084–95.
58. Nguyen AQ, Dela Cruz JA, Sun Y, Holmes TC, Xu X. Genetic cell targeting uncovers specific neuronal types and distinct subregions in the bed nucleus of the stria terminalis. J Comp Neurol. 2016;524:2379–99.
59. Gray JM, Vecchiarelli HA, Morena M, Lee TT, Hermanson DJ, Kim AB, et al. Corticotropin-releasing hormone drives anandamide hydrolysis in the amygdala to promote anxiety. J Neurosci. 2015;35:3879–92.
60. Reyes BAS, Carvalho AF, Szot P, Kalamarides DJ, Wang Q, Kirby LG, et al. Cortical adrenoceptor expression, function and adaptation under conditions of cannabinoid receptor deletion. Exp Neurol. 2017;292:179–92.
61. Natividad LA, Buczynski MW, Herman MA, Kirson D, Oleata CS, Irimia C, et al. Constitutive increases in amygdalar corticotropin-releasing factor and fatty acid amide hydrolase drive an anxious phenotype. Biol Psychiatry. 2017;82:500–10.
62. Henckens MJ, Deussing JM, Chen A. Region-specific roles of the corticotropin-releasing factor-urocortin system in stress. Nat Rev Neurosci. 2016;17:636–51.
63. Ramot A, Jiang Z, Tian JB, Nahum T, Kuperman Y, Justice N, et al. Hypothalamic CRFR1 is essential for HPA axis regulation following chronic stress. Nat Neurosci. 2017;20:385–8.
64. Sink KS, Walker DL, Freeman SM, Flandreau EI, Ressler KJ, Davis M. Effects of continuously enhanced corticotropin releasing factor expression within the bed nucleus of the stria terminalis on conditioned and unconditioned anxiety. Mol Psychiatry. 2013;18:308–19.
65. Silberman Y, Winder DG. Emerging role for corticotropin releasing factor signaling in the bed nucleus of the stria terminalis at the intersection of stress and reward. Front Psychiatry. 2013;4:1–12.
66. Zhou JN, Hofman MA, Gooren LJ, Swaab DF. A sex difference in the human brain and its relation to transsexuality. Nature. 1995;378:68–70.

ACKNOWLEDGEMENTS

The authors would like to thank Prof.Dr. Paul J. Lucassen (University of Amsterdam, The Netherlands) for editing the manuscript and providing helpful suggestions; Dr. Troy A. Roepke (Rutgers University, NJ, USA), Dr. Tao Zhang (Johns Hopkins University School of Medicine, MD, USA), Dr. Li-Feng Zhang (PKU-Nanjing Institute of Translational Medicine, Nanjing, China), and Prof. Guang-Hui Wang (Soochow University, Suzhou, China), for technical consultation; and thank Mr. Zhen-Bang Liu; Dr. Hui Fang; Dr. Chuan Huang; Dr. Xin-Ya Qin; Dr. Chen-Wei Wang; Dr. Gao Wu; (all from USTC); Mr. Meng-Cheng Huang (Shanghai Applied Protein Technology Co. Ltd, Shanghai, China); and Dr. Hui Gong (Huazhong University of Science and Technology, Wuhan, China) for technical support. We thank Dr. Wu Zhang and Mr. Hong-Jun Liu from Brain VTA ltd (Wuhan, China) for consultation of virus information. We thank Dr. Minmin Luo (NIBS Institute, Beijing, China) for providing the Ai14-reporter mice line. We also thank Dr. Yan-Yan Su from Anhui Medical University for graphical assistance.

AUTHOR CONTRIBUTIONS

PH and JNZ conceptualized the study. PH and YW designed experiments. PH and YW conducted experiments and analyzed data. XHQ helped with cell culture and molecular experiments and analyzed data. QHS helped with electrophysiological recording and calcium imaging data analysis. ZHH and PC contributed reagents and provided transgenic mice line. XM helped with calcium imaging data analysis. YPY and ZZ contributed reagents and provided helpful suggestions to the manuscript. PH wrote the paper together with JNZ with inputs from all co-authors. DFS, BAS and ZZ edited and revised the manuscript and provided helpful suggestions. All authors have read and approved the final version of the manuscript.

FUNDING

This work was supported by National Science Foundation of China (Grant No. 32030046; 32000716; 82271554; 82201671), the Strategic Priority Research Program of the Chinese Academy of Science (Grant No. XDB32020200), the National Key R&D Program of China (Grant No. 2022ZD0205202), the Key Direction Cultivation Funding from the University of Science and Technology of China (Grant No. WK3460000007).

COMPETING INTERESTS

The authors declare no competing interests.

ADDITIONAL INFORMATION

Supplementary information The online version contains supplementary material available at https://doi.org/10.1038/s41380-023-02144-6.

Correspondence and requests for materials should be addressed to Pu Hu or Jiang-Ning Zhou.

Reprints and permission information is available at http://www.nature.com/reprints

Publisher's note Springer Nature remains neutral with regard to jurisdictional claims in published maps and institutional affiliations.

Springer Nature or its licensor (e.g. a society or other partner) holds exclusive rights to this article under a publishing agreement with the author(s) or other rightsholder(s); author self-archiving of the accepted manuscript version of this article is solely governed by the terms of such publishing agreement and applicable law.